Langmuir

ARTICLE

pubs.acs.org/Langmuir

Phase Transitions and Spatially Ordered Counterion Association in Ionic-Lipid Membranes: Theory versus Experiment

V. B. Henriques,*[,†] R. Germano,[†,§] M. T. Lamy,[†] and M. N. Tamashiro*[,‡]

[†]Instituto de Física, Universidade de São Paulo, Caixa Postal 66318, 05314-970 São Paulo, SP, Brazil

[‡]Instituto de Física "Gleb Wataghin", Universidade Estadual de Campinas—UNICAMP, 13083-970 Campinas, SP, Brazil

ABSTRACT: Aqueous dispersions of phosphatidylglycerol (PG) lipids may present an anomalous chain-melting transition at low ionic strengths, as seen by different experimental techniques such as calorimetry or light scattering. The anomaly disappears at high ionic strengths or for longer acyl-chain lengths. In this article, we use a statistical model for the bilayer that distinguishes both lipid chain and headgroup states in order to compare model and experimental thermotropic and electrical properties. The effective van der Waals interactions among hydrophobic chains compete with the electrostatic repulsions between polar headgroups, which may be ionized (counterion dissociated) or electrically neutral (associated with counterions). Electric degrees of freedom introduce new thermotropic charge-ordered phases in which headgroup charges may be spatially ordered, depending on the electrolyte ionic strength, introducing a new rationale for experimental data on PGs. The thermal phases presented by the model for different chain lengths, at fixed ionic strength, compare well with an experimental phase diagram constructed on the basis of differential scanning calorimetry profiles. In the case of dispersions of DMPG (dimyristoyl phosphatidylglycerol) with added monovalent salt, the model properties reproduce the main features displayed by data from differential scanning calorimetry as well as the characteristic profile for the degree of ionization of the bilayer surface across the anomalous transition region, obtained from the theoretical interpretation of electrokinetic (conductivity and electrophoretic mobility) measurements.

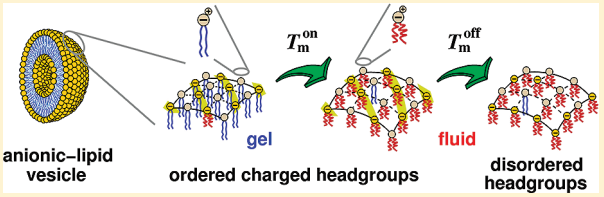

1. INTRODUCTION

Most model membranes composed of zwitterionic (neutral) phospholipids, such as PC (phosphatidylcholine), present a sharp gel−fluid (order−disorder) transition related to the disordering of the apolar hydrocarbonic chains, usually called the main transition.[1−6] A wealth of data and the corresponding rationale are available for this class of model lipid membranes. Much less is established with respect to charged-lipid model membranes.[7,8]

The numerous papers on the topic attest to the vital importance of the lipid-chain packing to membrane function[9] and drug development.[10] The possible relevance of chain melting in relation to the permeability of membranes to ions and small molecules, through the formation of lipid pores,[11] and the relation to protein channels is an open question.[12] The melting regime has been thoroughly investigated, both experimentally and theoretically, for neutral lipids. However, in spite of the large amount of data on charged-lipid membranes,[7,8] a satisfactory microscopic theory has not yet, to our knowledge, been given. Because the anionic phospholipid PG (phosphatidylglycerol) and its dimerized form, DPG (diphosphatidylglycerol, also called cardiolipin), constitute the major components of the cytoplasmic membranes in Gram-positive bacteria,[13] as, for example, in *Staphylococcus aureus*, we understand that filling this gap is of primary interest.

The chain melting of charged-lipid bilayers may display some peculiar properties. In the case of lipids containing polar headgroups that may undergo ionic dissociation such as anionic PG,[14] the main transition may be followed by anomalous profiles of various properties, depending on the acyl-chain length, lipid concentration, pH, and ionic strength, as seen from several experimental techniques, such as small-angle X-ray scattering (SAXS),[15−18] electronic spin resonance (ESR),[19−21] fluorescence spectroscopy (FS),[22] light scattering (LS),[23−25] optical microscopy of giant vesicles,[16,17,24] electron microscopy (EM),[26−28] and differential scanning calorimetry (DSC).[24−30] The anomalous behavior may extend through a range of temperatures. Henceforth, we shall refer to this wide thermal interval as the anomalous transition region (ATR).

To understand the origin of this peculiar behavior in PGs, it is natural to consider, preliminarily, the topology of the spontaneously formed anionic-lipid aggregates, in view of the rich polymorphism that may be observed in single-component as well as in mixed-lipid aqueous dispersions.[31] It has been experimentally established[32,33] that the self-assembled supramolecular structures of the saturated diacyl phospholipids depend on the hydrophobic acyl-chain length and on the polar headgroup. As an ordinary rule, short-chain homologues of these lipids form micelles, which in turn may be spherical or cylindrical, whereas longer-chain homologues form bilayers. In the specific case of the saturated diacyl anionic PGs, the shortest acyl-chain length that

Received: June 20, 2011
Revised: August 8, 2011
Published: August 17, 2011

supports bilayer structures corresponds to DLPG[33] (12 carbon atoms long[34]). Extensive studies on the DMPG ATR[14,22,24,35,36] confirm this general picture, providing experimental support for the stability of closed-bilayer aggregates. Henceforth, we will assume that sufficiently long acyl chain PGs in aqueous dispersions self-assemble, even along the ATR, in unilamellar vesicles.

The presence of charge undeniably plays a role in the thermal behavior of these systems. For low ionic strengths, this wide ATR is observed in the case of saturated diacyl anionic lipids of sufficiently short acyl-chain lengths, such as DLPG and DMPG, whereas for lipids of longer chains, such as DPPG, it becomes very narrow[27,37−39] and disappears completely for still longer chains, as in the case of DSPG. Additionally, DSC and LS data show that the behavior of zwitterionic lipid aqueous dispersions is recovered at high-ionic-strength conditions.[8,14,27,40−43] The salt screening and its effect on the aggregation behavior is well known in the case of micelles,[44,45] although ion-specific effects also come into play.[46] Furthermore, experiments on the conductivity of DMPG aqueous suspensions show substantial increases in the region of the broadened DSC peak,[23,30] which constitutes a strong indication of the important role played by charges in the ATR.

Coulomb interactions have been considered in the study of the phase polymorphism of charged-lipid lyotropic phases.[47,48] Harries et al.[49] have analyzed the transition between two fluid phases of charged multilamellar systems, treating the coupling among the lateral and the electric degrees of freedom through a model free energy comprising mean-field electrostatic and phenomenological nonelectrostatic interactions. A similar analytical treatment of these systems, combined with numerical simulations, has been performed by Jho et al.[50] However, previous attempts to explain the ATR of aqueous suspensions of ionic dissociating lipids[16,22,24,27,51] have been, except for ref 51 only qualitative, and none have taken into account the role of charges explicitly. Thus, to our knowledge, a fully statistical mechanical treatment of charge effects on the order−disorder transition of ionic-lipid model membranes has not yet been considered.

Electrostatic effects have been considered in the investigation of the role of the proton concentration, that is, the pH dependence, in phase transitions and the titration of anionic-lipid membranes.[52−55] Most of this work, however, is based on the Gouy−Chapman model[56,57] of the diffuse electric double layer, representing the Poisson−Boltzmann framework[58] applied to the planar case, in which the lipid membrane is treated as a uniformly charged surface in electrochemical equilibrium with an electrolyte solution consisting of pointlike ions in a continuum dielectric medium. The membrane protonation is taken into account by including a Stern layer[59] of adsorbed or lipid-bound protons. However, it has been known for some time[53] that this continuum approach of the surface charges cannot explain all relevant data, the rationale of which requires taking into account the discrete nature of the counterion adsorption to the acidic headgroups.

Besides protonation, considerable evidence has been given for monovalent inorganic ion adsorption to the lipid headgroups, in particular, the adsorption of the Na^+ counterion to the acidic headgroups. Earlier work on the role of pH[52,55] and later work on the effects of the acyl-chain length[43] have assumed no Na^+ binding to anionic phospholipids in aqueous suspensions. This association, however, which is more evident at high pH and in the absence of divalent counterions, has been supported by the analysis of atomistic simulations on PSs[60] and PGs[61] as well as by the theoretical interpretation of experimental measurements obtained by several independent techniques: nuclear magnetic resonance,[62] surface potential, lateral pressure and titration on monolayers,[63−65] electrophoretic mobility,[66,67] osmotic stress,[68] X-ray diffraction,[68−70] EM,[41,70] DSC,[41,69−72] ESR,[19,20,71,73] LS,[74,75] FS,[75] forces between Langmuir−Blodgett films via a force-measurement apparatus,[76] infrared spectroscopy,[77] and atomic force microscopy (AFM).[78] The counterion adsorption to the charged membrane can be treated by combining a Langmuir isotherm with the Gouy−Chapman theory,[79] although the microscopic interpretation of the apparent binding constant is a controversial issue.[80] According to Lyklema,[81] there are two almost independent communities that treat the aqueous−electrolyte interfacial problems with "chemical" or "physical" approaches. More recently, statistical mechanical models were introduced that were aimed at the calculation of the counterion binding constants to the charged headgroups.[63,82]

The chain melting for neutral-lipid model membranes has been analyzed in the theoretical literature in terms of a multiply degenerate two-state statistical model.[83−87] The model has also been successful in reproducing transitions of lipid mixtures[88,89] and has been used recurrently for different systems and properties,[12,90] such as permeability and membrane−cholesterol or membrane−protein interactions in the case of single-lipid membranes or of domain structure in the case of mixtures. The adequacy of a two-state model has gained support from a thermal and structural study by Nielsen et al.,[91] which strongly suggests an Ising universality-class critical behavior for the phase transitions.

Evidence for counterion adsorption on lipid headgroups led us to propose a generalization of the two-chain states statistical model for neutral-lipid membranes, to which we added ionized and counterion-reassociated headgroup states.[92] Because of the electrostatic repulsion among charged lipid headgroups, the ionized (counterion-dissociated) state favors the thermodynamic disordered acyl-chain fluid phase. Thus, the Coulomb interaction competes with the effective van der Waals attractions, which favor the thermodynamic ordered acyl-chain gel phase. Therefore, one might expect the lipids to become counterion-associated in the gel phase in order to make the area per headgroup small, whereas the fluid phase may allow counterion release to the surrounding aqueous solution. The result should depend on the ionic strength because the presence of salt screening implies a weakening of the electrostatic repulsion among charged headgroups and also renders additional counterions available to adsorption on the lipid surface. The coupling between the acyl-chain conformation and headgroup-charge degrees of freedom yields new thermodynamic phases in which headgroup charges may become spatially ordered under temperature variation or added monovalent salt. The checkerboard-like ordering of charged and neutral lipids gives rise to charge-ordered phases in which dissociated lipid headgroups form a regular pattern on the membrane surface. An inspection of the theoretical model calorimetric and ionization properties suggests that the experimentally observed ATR represents a manifestation of the existence of these novel thermotropic charge-ordered phases.

The purpose of this study is to investigate the thermodynamic properties of the theoretical model proposed previously[92] in the region of interest for comparison with experimental data on the thermal transitions of aqueous suspensions of the anionic PGs. In

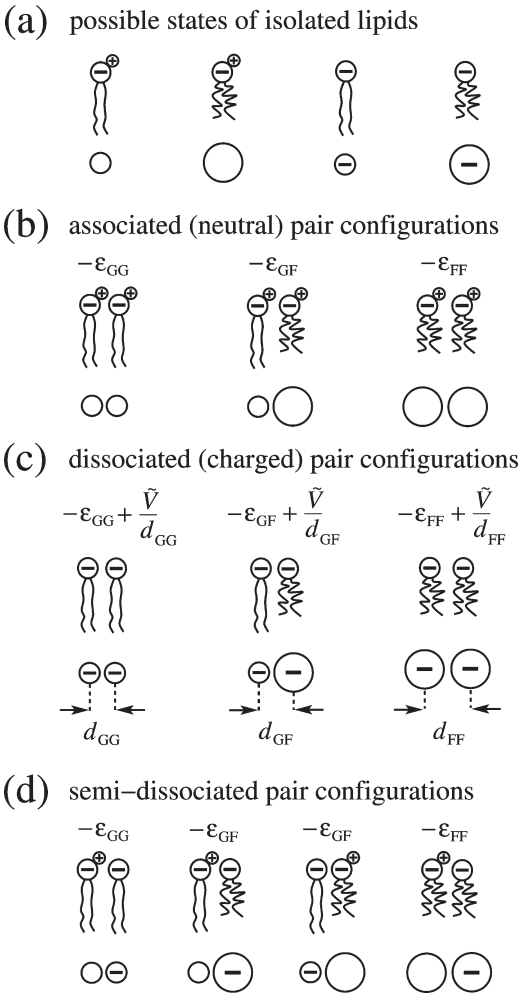

Figure 1. (a) Possible states of individual lipid molecules together with configurations of nearest-neighbor pairs of lipids and their effective pairwise energy contributions to the model energy $U = uN$ (eq 2) in each case: (b) pairs of counterion-bound (uncharged) lipid headgroups; (c) pairs of counterion-detached (charged) lipid headgroups, where the cationic counterions desorbed from the acidic headgroups and released to the surrounding aqueous solution are not shown; and (d) pairs of neutral and charged lipid headgroups; although one of the headgroups is charged, there is no additional Coulomb repulsion; the pairwise interaction energies are the same as in part b. We also show a schematic top-view representation of the lipid headgroups, to be used later in Figures 3, 5 and 8, to identify the distinct thermodynamic phases: a large empty circle represents a fluid acyl-chain lipid, a small empty circle corresponds to a gel acyl-chain lipid, and an internal minus sign represents a charged (dissociated or counterion-detached) anionic lipid headgroup. Counterion association leading to a neutral lipid headgroup is represented by an empty circle without the minus sign.

the case of DMPG, we compare model and experimental features for calorimetric and electrical properties. In section 2, we review the statistical model for ionic-lipid membranes proposed previously[92] in appropriate language for clearness, and we also introduce the thermal phases displayed by the model. Our main results are presented in section 3, in which the model phase properties are compared with those of PG suspensions, and in the particular case of DMPG, model features are analyzed with reference to calorimetric data as well as conductivity and electrophoretic mobility measurements of the lipid aqueous dispersions in the presence of monovalent salt. Some concluding remarks are presented in section 4.

2. STATISTICAL MODEL AND THERMODYNAMICS: CHAIN AND HEADGROUP CHARGE ORDERING

One may wonder what is the role of electrostatic interactions, if added to hydrophobic and "entropic" acyl-chain effects? The effective hydrophobic attractive interaction favors the gel (acyl-chain-ordered) phase at low temperatures, whereas the entropy of the disordered chains favors the fluid (acyl-chain-disordered) phase at higher temperatures. Electrostatic repulsions among ionized lipid headgroups drive them apart, thus favoring the fluid phase. Thus, the presence of charge should lower the main transition temperature,[94] when compared to that of a homologue chain-length zwitterionic lipid. However, a new scenario arises: the possibility of headgroup charge ordering on the membrane surface. The checkerboard-like ordering of charged and neutral lipids lowers both the energy and entropy, giving rise to a semidissociated (charge-ordered) gel phase at low temperatures, despite the Coulomb repulsion. The investigation of the consequences of the presence of charge requires that we look at a model for these competing interactions, hydrophobic attractions versus electrostatic repulsions.

We propose a model for ionic-lipid membranes in which lipids on a square lattice[95] may have their acyl chains disordered, whereas ionizable monovalent acidic groups on the lipid heads may dissociate and release cationic counterions into the surrounding aqueous solution. We thus consider only ionogenic[97] membranes that may reassociate with a single monovalent counterion at most. Thus, each lipid molecule has four possible states, characterized by the acyl-chain and the headgroup states. As depicted in Figure 1a, besides the usual (neutral) gel and fluid chain states, lipid headgroups may be charged (counterion-dissociated) or uncharged (counterion-associated). The effective cross-sectional areas per lipid a_F and a_G for the fluid and gel states satisfy $a_F > a_G$, as represented schematically by the large and small empty circles in the lower part of Figure 1a, corresponding to a top view of the lipid headgroups on the membrane.

Accordingly, lipid interactions are of two species: to the usual effective hydrophobic attractive interactions among acyl chains we add Coulomb repulsions between ionized headgroups. Pair energies are illustrated in Figure 1b–d. Hydrophobic interactions are described through effective parameters ε_{XY} for X, Y indicating, individually, either gel (G) or fluid (F) states.

The Coulomb repulsions for the ionized headgroups are treated in terms of an electrostatic potential energy $V = \tilde{V}/d_{ij}$, dependent on the intermolecular distance d_{ij}, with strength

$$\tilde{V} \equiv \frac{e^2}{4\pi\varepsilon_0\varepsilon_W} \tag{1}$$

where e is the electron charge, ε_0 is the permittivity of the vacuum, and ε_W is the water dielectric constant. As represented schematically in Figure 1c, the distance d_{ij} depends on the state of the neighboring lipid particles and is taken as $d_{GG} = (a_G)^{1/2}$, $d_{FF} = (a_F)^{1/2}$, or $d_{GF} = [(a_G)^{1/2} + (a_F)^{1/2}]/2$ for nearest-neighbor pairs in the gel–gel, fluid–fluid, or gel–fluid states, respectively.

The model energy density per lipid,[101] $u \equiv U/N$, for a membrane containing N lipid molecules, including all of the effective interaction

energies presented in Figure 1b−d, is

$$u = -\varepsilon_{GG}n_{GG} - \varepsilon_{FF}n_{FF} - \varepsilon_{GF}n_{GF} + \tilde{V}\left(\frac{n_{GG}^{--}}{d_{GG}} + \frac{n_{FF}^{--}}{d_{FF}} + \frac{n_{GF}^{--}}{d_{GF}}\right) \quad (2)$$

where n_{XY} is the number density of lipid pairs in the XY pair states, regardless of their headgroup charge states, with XY = gel−gel, fluid−fluid or gel−fluid and n_{XY}^{--} being the analogous number density when both lipids in the pair are charged. We thus consider only the electrostatic interactions among nearest-neighbor pairs of charged lipid headgroups, neglecting the contributions arising from charged-lipid pairs located at longer separations.

The model lipid surface may suffer area changes as well as ionization variations depending on the temperature T and bulk salt concentration. Thus, we need to introduce the membrane area per lipid

$$a = n_G a_G + n_F a_F = a_F - n_G \Delta a, \quad \Delta a \equiv a_F - a_G > 0 \quad (3)$$

in which n_G and n_F are, respectively, the number densities of gel and fluid particles regardless of their headgroup charge states and the membrane surface charge number density (or degree of dissociation)

$$\alpha = n_G^- + n_F^- \quad (4)$$

in which n_G^- and n_F^- are, respectively, the number densities of charged gel and charged fluid particles.

To obtain the model thermal properties, one must sum over all possible acyl-chain and headgroup lipid states. In this case, it is easier to obtain the statistical properties by considering the lipid membrane under an external applied lateral pressure Π and in contact with a reservoir of counterions. The latter represents the electrolytic aqueous solvent and may be described through the counterion chemical potential μ_c. Thus, the counterion chemical potential, which is dependent on the quantity of added salt, controls the density of adsorbed (or lipid-bound) counterions, n_b, which partially neutralize the otherwise fully charged lipid headgroups on the membrane. Co-ion adsorption is neglected because of the strong electrostatic repulsion among the charged acidic headgroups and the like-charged anionic co-ions. The adsorbed counterion density n_b is complementary to the density of charged lipids on the membrane and thus must satisfy the normalization condition

$$n_b + n_G^- + n_F^- = n_b + \alpha = 1 \quad (5)$$

The fewer counterions that are associated at the lipid membrane, the larger the number of remaining ionized headgroups and the net surface charge of the membrane with N lipids, $Q = -N\alpha|e|$, which yields a net surface charge density of $\sigma = -\alpha|e|/a$.

Area and surface charge are controlled, respectively, through lateral pressure Π and counterion chemical potential μ_c and compose part of the appropriate thermodynamic potential per particle, which is written as

$$\psi(T, \Pi, \mu_c) = \langle u - Ts + \Pi a - \mu_c n_b \rangle \quad (6)$$

where s is the model entropy per lipid and the brackets denote ensemble averages, defined below. This potential is obtained from the calculation of the associated partition function $\Xi_N(T, \Pi, \mu_c) = \exp[-\beta N \psi(T, \Pi, \mu_c)]$, which reads

$$\Xi_N(T, \Pi, \mu_c) = \sum_{\{X\}} \omega^{N(1-n_G)} \exp[-N\beta(u + \Pi a - \mu_c n_b)] \quad (7)$$

with $\beta \equiv (k_B T)^{-1}$ and $\Sigma_{\{X\}}$ denoting a trace over all possible 4^N lipid acyl-chain and lipid headgroup configurations $\{X\}$. In this expression, the entropy associated with the lipid acyl-chain rotamers of the disordered fluid state is decoupled from other degrees of freedom. Parameter ω represents the highly degenerate configurations of the diacyl chains in the fluid state of a single lipid molecule. The ensemble averages of any observable $\mathcal{O}$ are also calculated with the same Boltzmann−Gibbs factors,

$$\langle \mathcal{O}(\{X\}) \rangle \equiv \frac{1}{\Xi_N} \sum_{\{X\}} \mathcal{O}(\{X\}) \omega^{N(1-n_G)} \times \exp[-N\beta(u + \Pi a - \mu_c n_b)] \quad (8)$$

To establish the possible ordered phases presented by the model system, it is interesting to analyze the ground-state potential (eq 6) at zero temperature $\psi(T = 0, \Pi, \mu_c)$, as illustrated in Figure 4 of ref 92. It is convenient to define the dimensionless thermodynamic parameters and interaction energies as

$$\lambda \equiv \frac{d_{FF}}{d_{GG}} = \sqrt{\frac{a_F}{a_G}} > 1, \; J \equiv \varepsilon_{GG} + \varepsilon_{FF} - 2\varepsilon_{GF} > 0,$$
$$t \equiv \frac{k_B T}{J} > 0, \; \mu \equiv \frac{\mu_c}{J}, \; \upsilon \equiv \frac{4\tilde{V}}{J d_{FF}} > 0,$$
$$p \equiv \frac{2\Pi\Delta a + \Delta\varepsilon}{4J}, \; \Delta\varepsilon = 4(\varepsilon_{GG} - \varepsilon_{FF}) > 0 \quad (9)$$

The analysis yields six stable phases: at high salt content, $\mu > 0$, the usual gel and fluid phases for a neutral membrane are predicted. These two usual phases are characterized by $n_G = 1$, $n_G^- = 0$ and $n_F = 1$, $n_F^- = 0$, respectively. At very low ionic strength, $\mu < -\upsilon$, $\mu < -4p - \upsilon$, or $\mu < -\lambda\upsilon$ (depending on the p value, see Figure 4 of ref 92), the gel and fluid phases occur for a fully charged membrane with $n_G = 1$, $n_G^- = 1$ and $n_F = 1$, $n_F^- = 1$, respectively. For intermediate added salt concentration, new gel and fluid phases for a membrane with charge-ordered headgroups arise. Charged headgroups organize in a checkerboard fashion, and the corresponding densities are $n_G = 1$, $n_G^- = {}^1/_2$ for the gel charge-ordered phase, and $n_F = 1$, $n_F^- = {}^1/_2$ for the fluid charge-ordered phase. The more ordered gel phases of the three distinct types (associated neutral, semidissociated charge-ordered, and fully dissociated) are present at high enough lateral pressure, as expected. For lipid monolayers, most of the low-temperature fluid-phase region may be considered to be unphysical because it corresponds to negative values for the lateral pressure Π.

The model system thermal properties may be obtained through a mean-field Bragg−Williams approximation.[102,103] This consists of writing the number densities of lipid pairs $\{n_{XY}\}$ and $\{n_{XY}^{--}\}$ in terms of the number densities of isolated lipids $\{n_X\}$ and $\{n_X^-\}$, that is, by neglecting pair correlations and writing

$$n_{XY} = 2(n_X\langle n_Y\rangle + \langle n_X\rangle n_Y - \langle n_X\rangle\langle n_Y\rangle)$$
$$n_{XY}^{--} = 2(n_X^-\langle n_Y^-\rangle + \langle n_X^-\rangle n_Y^- - \langle n_X^-\rangle\langle n_Y^-\rangle) \quad (10)$$

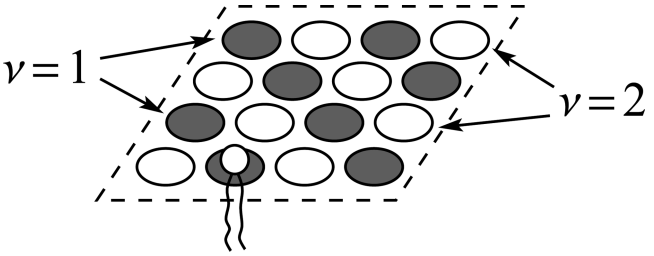

Figure 2. Schematic representation of a small portion of one leaflet of a bilayer membrane, displaying its subdivision in two interpenetrating square sublattices, labeled by $\nu = 1$ (shaded sites) and $\nu = 2$ (unshaded sites). So as not to overcrowd the figure, only one of the lipid molecules that comprise the monolayer was drawn. Assuming only nearest-neighbor pairwise interactions, a lipid in the $\nu = 1$ sublattice interacts only with neighboring lipids in the $\nu = 2$ complementary sublattice.

where the factor of 2 represents half of the coordination number $\gamma = 4$ of the square lattice. Note that under this approach the effective model energy per lipid, $u - k_B T(1 - n_G) \ln \omega + \Pi a - \mu_c n_b$, becomes linear in lipid densities $\{n_X\}$ and $\{n_{\bar{X}}\}$, which allows an exact evaluation of the partition function (eq 7) and of the ensemble averages (eq 8). Therefore, under this mean-field approximation, a particular microstate $\boldsymbol{X}$ of the model system is defined through variables n_G, $n_{\bar{F}}$, and $n_{\bar{G}}$, which are the overall density of particles in the gel state and the densities of charged particles in the fluid and gel states, respectively. The number density of acyl chains in the fluid state is given by $n_F = 1 - n_G$ because of particle conservation.

To obtain a mathematical description of the checkerboard-like charge-ordered headgroup phases, it is necessary to divide the planar membrane into two interpenetrating sublattices, as depicted in Figure 2 for the square lattice. The two sublattices are indexed as $\nu = 1$ and 2, and the pair number densities in eq 2 must be replaced by

$$n_{GG} \rightarrow n_{G_1G_2},\ n_{FF} \rightarrow n_{F_1F_2},\ n_{GF} \rightarrow n_{G_1F_2} + n_{F_1G_2} \tag{11}$$

with analogous expressions for $\{n_{\bar{X}\bar{Y}}\}$, after which one may proceed with the Bragg–Williams approximation (eq 10) in terms of the lipid densities $\{n_{X_\nu}\}$ and $\{n_{\bar{X}_\nu}\}$ in each sublattice. The average surface-charge density $\langle\alpha\rangle$ is defined on each sublattice through parameters $\langle\alpha\rangle_1$ and $\langle\alpha\rangle_2$. Charged headgroup order is then present for $\langle\alpha\rangle_1 \neq \langle\alpha\rangle_2$. The division of the lipid surface into sublattices also introduces the sublattice averages for chain states, described through $\langle n_G\rangle_\nu$ and for the remaining densities that define the thermodynamic state, $\langle n_{\bar{F}}\rangle_\nu$ and $\langle n_{\bar{G}}\rangle_\nu$. These are formally defined by eq 8 applied to observables n_{G_ν}, $n_{\bar{F}_\nu}$, and $n_{\bar{G}_\nu}$ on sublattice ν, respectively.

Standard statistical mechanical methods presented in detail elsewhere[92] yield the following molecular thermodynamic free-energy functional[104] for lipids on a square lattice

$$\begin{aligned}\frac{1}{J}\psi = &-\mu - \frac{2\varepsilon_{FF}}{J} + \frac{\Pi a_F}{J} - t\ln\omega + 2\langle n_G\rangle_1\langle n_G\rangle_2 \\ &- \frac{t}{2}\sum_{\nu=1,2}\ln\xi_\nu - \frac{\upsilon}{2}\Big[\langle n_{\bar{F}}\rangle_1\langle n_{\bar{F}}\rangle_2 + \lambda\langle n_{\bar{G}}\rangle_1\langle n_{\bar{G}}\rangle_2 \\ &+ \frac{2\lambda}{1+\lambda}\left(\langle n_{\bar{F}}\rangle_1\langle n_{\bar{G}}\rangle_2 + \langle n_{\bar{G}}\rangle_1\langle n_{\bar{F}}\rangle_2\right)\Big]\end{aligned} \tag{12}$$

with dimensionless parameters defined by eq 9. The single-site effective partition function of sublattice $\nu = 1$ reads

$$\xi_1 \equiv \sum_{\{\boldsymbol{x}\}\in\nu=1} e^{\beta\phi_{\boldsymbol{x}}^{(1)}} \tag{13}$$

with associated Boltzmann weights $\beta\phi_{\boldsymbol{x}}^{(1)}$ given by

$$\beta\phi_{F^0}^{(1)} = 0 \tag{14}$$

$$\beta\phi_{G^0}^{(1)} = \frac{2p}{t} + \frac{2(2\langle n_G\rangle_2 - 1)}{t} - \ln\omega \tag{15}$$

$$\beta\phi_{F^-}^{(1)} = -\frac{\mu}{t} - \frac{\upsilon}{t}\left(\langle n_{\bar{F}}\rangle_2 + \frac{2\lambda}{1+\lambda}\langle n_{\bar{G}}\rangle_2\right) \tag{16}$$

$$\beta\phi_{G^-}^{(1)} = \beta\phi_{G^0}^{(1)} - \frac{\mu}{t} - \frac{\lambda\upsilon}{t}\left(\langle n_{\bar{G}}\rangle_2 + \frac{2}{1+\lambda}\langle n_{\bar{F}}\rangle_2\right) \tag{17}$$

where Boltzmann weight indices F^0, G^0, F^-, and G^- indicate the four possible states $\{\boldsymbol{x}\}$ of a single lipid: a neutral fluid, a neutral gel, a charged fluid, and a charged gel, respectively. The single-site effective partition function ξ_2 of sublattice $\nu = 2$ is obtained by switching the sublattice labels $1 \rightarrow 2$ and $2 \rightarrow 1$ in eqs 13–17. The method also leads to the following equations of state for sublattice $\nu = 1$ averages for lipid-chain order, charged-headgroup fluid order, and charged-headgroup gel order:

$$\langle n_G\rangle_1 = \frac{e^{\beta\phi_{G^0}^{(1)}} + e^{\beta\phi_{G^-}^{(1)}}}{\xi_1},\ \langle n_{\bar{F}}\rangle_1 = \frac{e^{\beta\phi_{F^-}^{(1)}}}{\xi_1},\ \langle n_{\bar{G}}\rangle_1 = \frac{e^{\beta\phi_{G^-}^{(1)}}}{\xi_1} \tag{18}$$

The equations of state for the thermal self-averages of sublattice $\nu = 2$ are obtained by switching the sublattice labels $1 \rightarrow 2$ and $2 \rightarrow 1$ in eqs 13–18.

A detailed presentation of the solution to eqs 13–18 and the respective analysis have been given elsewhere.[92] Different sets of thermal phases may be obtained depending on the model system parameters. In this study, our aim is to compare the thermodynamic model features with experimental results for aqueous dispersions of the anionic-lipid PGs in the presence of monovalent added electrolyte.[14,22,25–27,30] As discussed in the Introduction, PGs may display an ATR beyond the gel–fluid main transition, with anomalous specific-heat profiles,[14,24–30] low turbidity,[23,24] high electrical conductivity,[23,30] and high viscosity.[27,30] This experimental ATR and its associated properties disappear under the addition of salt[8,14,27,40–43] and are absent for long enough acyl chains,[27,37–39] for which the large hydrophobic attraction renders the electrostatic repulsion negligible.

Thus, our interest lies in model systems that present a low-temperature neutral gel state as well as the special charge-ordered gel and fluid phases. We therefore choose to look at high enough lateral pressure Π, so that the gel phase is the low-temperature phase with respect to acyl chains, and seek parameters that guarantee that the electrostatic repulsion $\tilde{V}/d_{XY}$ competes with the hydrophobic attraction J. General features of the model system thermal properties under the conditions we just described , i.e., $p > (\lambda - 1)\upsilon/4$ and large enough υ, are presented in Figure 3.

Figure 3 illustrates the possible phases at different ionic strengths μ of the lipid bilayer as reduced temperature t is varied. As can be seen in the figure, the presence of the lipid-chain

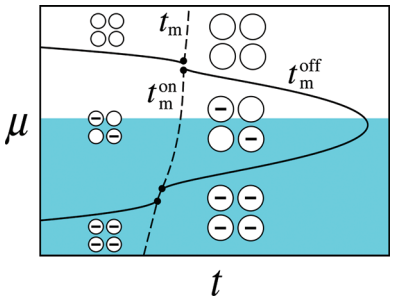

Figure 3. Typical mean-field phase diagram $\mu \times t$ for strong electrostatic−hydrophobic competition parameter υ, keeping parameters p, λ, and ω fixed. Solid lines are continuous transitions, whereas dashed lines represent discontinuous transitions. The small black circles represent critical end points, where lines of discontinuous transitions meet at the ending of a line of continuous transitions. The cartoons in the different regions of the phase diagram represent the headgroup and acyl-chain configurations of the corresponding ground-state structures using the schematic top-view representation introduced in Figure 1. As discussed in the main text, in the shaded region the charged bilayer is unstable; therefore, this portion of the phase diagram may be considered to be inaccessible and unphysical.

gel−fluid main transition (dashed line) is independent of ionic strength,[105] but its associated temperature t_m (or t_m^{on} for intermediate values of μ) decreases as the added salt concentration diminishes. This is in agreement with the experimental behavior for charged-lipid aqueous suspensions[14,22,25−27,30] and is to be expected[94] because in the absence of enough counterions the charged headgroups favor acyl-chain disordering.

Headgroup-charge order arises at intermediate ionic strengths: the main (chain) transition at t_m^{on} takes place inside the charge-ordered headgroup phase and is accompanied by an enhancement of surface charge, as will be shown later in Figure 6. Charged headgroups disorder at higher temperatures t_m^{off}, beyond the main transition at t_m^{on}. Thus, in this region of the ionic strength $\times$ temperature phase diagram, a sequence of two transitions[106] is seen as the temperature is raised: the main chain gel−fluid transition at t_m^{on}, with latent heat, and a smooth, continuous charge-disordering transition at t_m^{off}. As we suggest in the next subsection, this sequence of transitions might be a possible interpretation of the experimentally observed ATR of shorter-chain PGs at low ionic strength.[14] Note that the double transition disappears at higher salt concentrations, similar to that observed in experiments with aqueous suspensions of PGs.[8,14,27,40−43]

At still lower ionic strength, the membrane might be completely dissociated and the main chain transition takes place at comparatively lower temperatures, with no headgroup-charge order. The latter phases may, however, be physically inaccessible because the membrane structure may become unstable in the presence of excessive charge, as we argue below.

An important point to note is that a completely charged membrane with $n_G^- = 1$ might be unstable, depending on the value of υ. For the lipid aggregate, which constitutes the bilayer membrane, to exist, a net attractive model energy density u is needed. From eq 2, this requires $\varepsilon_{GG} > \tilde{V}/d_{GG}$ for the fully charged surface or equivalently (see the definitions in eq 9)

$$\frac{\varepsilon_{GG}}{J} > \frac{1}{4}\lambda\upsilon \tag{19}$$

However, if the net interaction $|u|$ is very small, then the charged membrane might disaggregate before the acyl chains disorder. In other words, for a gel−fluid transition to be present in the case of the $n_G^- = 1$ membrane, the transition temperature T_m should be lower than the disaggregation temperature T_{disag}, which is proportional to $|u|$. The latter relation may be obtained by a lattice-gas model[107] in which the fluid phase is associated with a void-rich, loosely packed state. The above reasoning allows us to consider the lower shaded portion of the phase diagram of Figure 3 to be unphysical.

3. COMPARISON OF RESULTS: THEORY × EXPERIMENTS

The charged-lipid aqueous dispersions of anionic PGs may present a broad DSC peak at low ionic strength, depending on the chain length.[27,37−39] When it is present, the broadening of the DSC peak reflects structural changes that, in turn, influence the optical as well as transport properties that also display anomalous properties in the transition region.

In the following text, we undertake a detailed comparative study of the thermal and electrical properties of the model system and those experimentally measured on aqueous suspensions of anionic-lipid DMPG in the presence of monovalent counterions.[14] The thermal behavior of the theoretical model depends on a set of five parameters: the ratio of the area per lipid headgroup in the fluid and gel phases $\lambda^2 \equiv a_F/a_G$, the fluid acyl-chain entropy ω, the effective hydrophobic interaction J, the effective lateral-pressure parameter p, and the ratio υ of the electrostatic to hydrophobic interaction parameters. The value of the lipid area ratio is well established for the zwitterionic PCs (Table 2 in Section 3.4) on the basis of estimates of their cross-sectional areas per lipid in the gel[108] and fluid[109] phases, $a_G = 47.3$ Å^2 and $a_F = 60$ Å^2, respectively, which yields $\lambda = 1.126$. For the remaining parameters, we proceed as follows: (i) the hydrophobic interaction parameter J, the chain entropy ω, and the effective lateral-pressure parameter p are obtained through fitting our model properties to ESR experimental data at high ionic strength, as described in the following subsection; (ii) the electrostatic−hydrophobic competition parameter υ is then estimated by considering monovalent acidic headgroups and the water dielectric constant. The phase diagram with estimated and fitted parameters is presented in section 3.2, and the description of membrane ionization and the specific-heat profile are given in section 3.3. After this detailed comparison with DMPG, we explore the effect of acyl-chain length on the ATR in section 3.4.

3.1. Estimation of the Model Parameters from ESR Experimental Data in the High-Ionic-Strength Limit. Here we estimate model parameters ω, J, and p from the thermotropic behavior of the DMPG aqueous dispersions in the regime of high salt concentration, for which the experimental system displays behavior entirely analogous to that of neutral membranes. In the latter case, the thermal phase of the theoretical model is described by the single order parameter $\langle n_G \rangle$, which is related to chain order and mobility.

From the standpoint of the theory, the limit of strong electrostatic screening corresponds mathematically to $\mu_\nu \to \infty$. In this limit, eqs 13−18 yield null membrane ionization, and the system is fully described by the single order parameter for the fraction of lipid chains in the gel state $\langle n_G \rangle$. Equations 18 with $\mu \to \infty$ yield $\langle n_F^- \rangle_\nu = \langle n_G^- \rangle_\nu = 0$ and

$$\langle n_G \rangle = \frac{1}{2}\left[1 + \tanh\left(\frac{2\langle n_G \rangle - 1}{t} + \frac{p}{t} - \frac{1}{2}\ln\omega\right)\right] \tag{20}$$

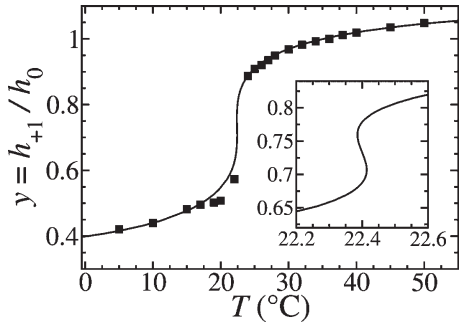

Figure 4. Temperature dependence of the ratio between the amplitudes of the low- and central-field resonance lines $y \equiv h_{+1}/h_0$ measured experimentally on the ESR spectra of 0.2 mol % 16-PCSL incorporated in 10 mM DMPG in 10 mM Hepes buffer at pH 7.4 and a high salt concentration of 100 mM NaCl (filled squares). The solid line represents the best nonlinear theoretical fitting by using eqs 20 and 22. The fitted values found are $y_{min} = 0.3448065$, $y_{max} = 1.12095647$, $\omega = 6708$, and $t_m \equiv t(T = 22.4\ °C) = 0.9953856$, with the two latter to be used in further calculations. The inset displays in more detail the region in the vicinity of the first-order transition at $T_m = 22.4\ °C$, associated with the presence of a characteristic van der Waals loop. Because the fitted reduced temperature t_m is very close to the critical one (at the mean-field level) of $t_{crit} = 1$, the van der Waals loop is hardly noticeable.

In this high-salt-content limit, the main transition temperature t_m between the $\langle n_G \rangle \neq 0$ gel phase and the $\langle n_G \rangle = 0$ fluid phase is related to the coexistence lateral-pressure parameter p_m through the relation

$$p_m = \frac{t_m}{2} \ln \omega \tag{21}$$

which can be deduced from an inspection of eq 20. The relevance of this relation as a check on the fitted parameters will be seen in the following text. Equation 20 also yields a limiting (critical) temperature $t_{crit} = 1$ at which the latent heat would become null. From a theoretical point of view, coexistence between the gel and fluid phases may be present up to the critical point $t_{crit} = 1$, beyond which phase transitions no longer occur.

In the case of monolayers,[63−65,99,100,110] this relation yields the lateral pressure Π_m at which headgroup areas change abruptly for a given temperature. For bilayer vesicles, the lateral pressure is not a controllable parameter, but its value at the transition may be obtained through theoretical modeling[111] and fitting to experimental data. There is evidence, however, that monolayers and bilayers are equivalent at a lateral pressure Π of between 30 and 35 mN/m,[112] which would correspond to the tension-free state normally found in extended lipid bilayers. This homology validates the use of a model that represents a single monolayer in order to describe the properties of unilamellar vesicles.

Experimentally, the fraction of lipids in the gel state $\langle n_G \rangle$ is not directly accessible. However, acyl-chain mobility is a related property that can be obtained by ESR measurements from spin labels incorporated into the lipid bilayer. There are several choices of experimental parameters to quantify this property, but a particular one adopted in previous work,[14,15] due to the accuracy of the measurements and its sensitivity, is the ratio $y \equiv h_{+1}/h_0$ between the amplitudes of the low-field and the central-resonance lines measured on the ESR spectra, as presented in Figure 4. A highly anisotropic ESR signal associated with small values of y indicates the predominance, in the bilayer, of lipids in the gel state, whereas an isotropic signal coupled to values of y close to unity can be explained by a higher mobility of the spin-label probe due to the major presence of lipids in the disordered fluid state.

We assume, for simplicity, a linear relationship between the theoretical fraction $\langle n_G \rangle$ and the experimental ratio y:

$$\langle n_G \rangle = 1 + \left(\frac{1}{1 + \omega} - 1 \right) \left(\frac{y - y_{min}}{y_{max} - y_{min}} \right) \tag{22}$$

This simple expression yields the expected asymptotic limits $\langle n_G \rangle \rightarrow 1$ for $y \rightarrow y_{min}$ (low temperatures) and $\langle n_G \rangle \rightarrow 1/(1 + \omega)$ for $y \rightarrow y_{max}$ (high temperatures).

Equations 20 and 22 are used to fit the experimental data measured on the ESR spectra of 0.2 mol % 16-PCSL incorporated into 10 mM DMPG in 10 mM Hepes buffer at pH 7.4 at a high salt concentration of 100 mM NaCl,[15] and the main transition temperature $T_m = 22.4\ °C$ is taken from DSC measurements.[14,15] The result of the fitting procedure is shown in Figure 4 and leads to the following set of best-fit parameters:[113] $y_{min} = 0.3448065$, $y_{max} = 1.12095647$, $\omega = 6708$, and $t_m \equiv t(T = 22.4\ °C) = 0.9953856$. It is noteworthy that the fitted reduced temperature of the transition t_m is very close and slightly below the critical temperature $t_{crit} = 1$, a fact that has been pointed out previously.[83,91,114] The gel−fluid coexistence lateral-pressure parameter p_m and dimensionless temperature t_m are related by eq 21, which yields $p_m = 4.38524$. In view of the evidence of the monolayer−bilayer equivalence at a lateral pressure in the restricted range of 30 mN/m < Π < 35 mN/m,[112] we assumed $p = p_m$ to be constant throughout the experiments.

The consistency of the above fit to the ESR data can be checked with independent measurements for the enthalpy obtained from calorimetric experiments. The Clapeyron equation[115] for the gel−fluid pressure−temperature coexistence line is written as

$$\left(\frac{d\Pi}{dT} \right)_{T_m} = \frac{\Delta H}{T_m \Delta a} \tag{23}$$

Applied to our expression for the coexistence pressure parameter p_m (eq 21), this yields a variation in enthalpy for the transition given by $\Delta H = k_B T_m \ln \omega$. Thus our fitting for the acyl-chain order parameter behavior to ESR data leads to a latent heat of the gel−fluid transition of $\Delta H_{fit} = k_B T_m \ln \omega \approx 5.175$ kcal/mol. This value may be compared to the transition enthalpy ΔH_{exp} obtained from DSC[14] for DMPG suspensions under high-ionic-strength conditions (100 mM NaCl), $\Delta H_{exp} = 5.7 \pm 0.8$ kcal/mol, which does not differ much from the data at low ionic strength (6 mM NaCl), $\Delta H_{exp} = 5.2 \pm 0.8$ kcal/mol. These values are consistent with the experimental data on homologue zwitterionic lipid suspensions,[5] more specifically, DMPC multilamellar vesicles and DMPC small (<100 nm) unilamellar vesicles that yield, respectively, $T_m = 23.6 \pm 1.5\ °C$, $\Delta H_{exp} = 6.0 \pm 2.4$ kcal/mol and $T_m = 22.2 \pm 2.0\ °C$, $\Delta H_{exp} = 4.1 \pm 0.9$ kcal/mol. All of these experimental estimates compare very well to the above value of enthalpy obtained from the independent fitting of eqs 20 and 22 to the ESR experimental data, $\Delta H_{fit} \approx 5.175$ kcal/mol.

3.2. DMPG Phase Diagram. Aqueous dispersions of anionic-lipid DMPG in the presence of monovalent added electrolyte[14] have been extensively investigated, and from the experimental data on calorimetric as well as optical, electrical, and viscosity

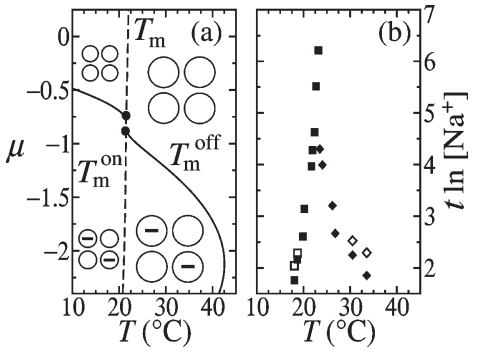

Figure 5. Comparison between (a) the theoretical mean-field phase diagram in the $\mu \times T$ plane for $p = 4.38524$, $\lambda = 1.126$, $\omega = 6708$, and $\upsilon = 4.2$ and (b) experimental ATR data for 10 mM DMPG in 10 mM Hepes buffer at pH 7.4 for several ionic strengths: T_m^{on} (■) and T_m^{off} (◆). The meaning of the symbols in part a is the same as described in the caption of Figure 3. Counterion number densities $[Na^+]$ in part b were normalized to 1 mM. Empty squares (□) and empty diamonds (◇) for the two lowest counterion concentrations are data considering the additional contributions arising from the DMPG partial dissociation, as explained in the main text.

properties, one may draw an ionic strength × temperature phase diagram. To compare it to the theoretical model phase diagram, besides the fitted values found in the previous subsection, we need to fix the fluid−gel area ratio λ as well as the electrostatic−hydrophobic competition parameter υ. For the area-ratio parameter, we set $\lambda \equiv (a_F/a_G)^{1/2} = 1.126$, as already explained in the introduction to this section. The choice of the electrostatic−hydrophobic competition parameter υ is more delicate because one may expect deviations from the bare unscreened Coulomb form $\upsilon_{bare} \equiv 4\tilde{V}/Jd_{FF} = 4t_m(l_B/d_{FF})(T_{room}/T_m)$, where $l_B \equiv e^2/(4\pi\varepsilon_0\varepsilon_W k_B T_{room}) \approx 7.15$ Å is the Bjerrum length[116] at room temperature $T_{room} = 298.15$ K. Thus, one obtains $\upsilon_{bare} \approx 3.7075$ by using the main transition temperature $T_m = 22.4$ °C taken from DSC measurements,[14,15] its fitted reduced value $t_m = 0.9953856$ from ESR data, and the estimate for the distance between headgroups in the fluid phase of DMPC,[109] $d_{FF} = (a_F)^{1/2} = 7.75$ Å; see also Table 2. However, among other neglected effects,[117] the local dielectric constant should be smaller than that of bulk water ε_W, so we set a somewhat higher value of $\upsilon = 4.2$, which allows the double transition to be present in the phase diagram, in accordance with the ATR of the experimental data.

Figure 5a displays the system dimensionless chemical potential of counterions $\mu \equiv \mu_c/J$ versus temperature T theoretical phase diagram for the above model parameters. For comparison, the DSC experimental data for the limits of the ATR, T_m^{on} and T_m^{off}, are presented in Figure 5b for different added monovalent salt (NaCl) concentrations. The data displayed in Figure 5b are reorganized from DSC measurements on DMPG at different ionic strengths.[123] The two limiting temperatures correspond to the temperature of the main DSC peak (T_m^{on}) and to the temperature at which the shoulder ends (T_m^{off}). In the graph, the two temperatures, T_m^{on} and T_m^{off}, are associated with the respective sodium ion concentration, which is represented in terms of the ideal gas expression for the chemical potential of counterions, $\mu \equiv \mu_c/J = t \ln [Na^+]$, where $[Na^+]$ is the counterion number density. At salt concentrations much higher than the anionic-lipid densities, there are two main contributions to the $[Na^+]$ counterion concentration: Na^+ ions come from added salt and from NaOH in buffer. Experiments were performed at different salt concentrations[123] and at 10 mM Hepes buffer at pH 7.4 (adjusted with 4 mM NaOH). The data (full symbols) displayed in Figure 5b are presented in Table 1.

Table 1. Temperature Range Associated with the ATR, $T_m^{on} < T < T_m^{off}$, Obtained from DSC Profiles for a 10 mM DMPG Aqueous Suspension in 10 mM Hepes Buffer at pH 7.4 and Several Nominal NaCl Concentrations[123]

NaCl (mM)	$[Na^+]$ (mM)[a]	T_m^{on} (°C)	T_m^{off} (°C)
2	6[b]	18.05	33.55
5	9[b]	18.7	30.5
10	14	19.9	26.8
20	24	20.2	26.2
50	54	21.7	24.05
70	74	21.95	23.5
100	104	22.4	
250	254	22.7	
500	504	23.2	

[a] Differences between the first and second columns are due to 4 mM NaOH present in the Hepes buffer at pH 7.4. [b] See also corrections to these values, due to DMPG partial dissociation, in the main text.

For the two lowest salt concentrations (2 and 5 mM NaCl), a second set of data was obtained (empty symbols in Figure 5b). The $[Na^+]$ concentration was calculated by adding counterions steming from the partial dissociation of DMPG, $[Na^+]_{ct} = [PG^-] = \langle\alpha\rangle[DMPG]$. This excess density was calculated from the profile of the experimental degree of ionization $\langle\alpha\rangle$ across the ATR obtained in ref 123 from conductivity and electrophoretic mobility data. By taking the product of the lipid density and the values of the degree of ionization at the two limiting temperatures, at each salt density, one obtains for 2 mM NaCl, $[Na^+] = 8$ mM at T_m^{on} and 9.2 mM at T_m^{off}, and for 5 mM NaCl, $[Na^+] = 10.2$ mM at T_m^{on} and 11.8 mM at T_m^{off}. These values are not shown in Table 1, but are plotted in Figure 5b: □ for T_m^{on} and ◇ for T_m^{off}. It can be seen that when the ion densities are comparable to or even smaller than the lipid concentrations, variations in the fraction of adsorbed counterions can lead to significant changes in the bulk counterion concentration.

The similarity between the two phase diagrams is remarkable: the main transition temperature T_m (in theory) and the onset of the ATR, T_m^{on} (in the experiment), increase slightly with salt concentration, whereas the temperature at which charge disorders (in the model), analogously with temperature T_m^{off} (in the experiment), associated with the end of the ATR, decreases less moderately. At higher salt concentrations, a single first-order transition between the neutral gel and the neutral fluid phases is present, both in theory and in the experiment.

3.3. Model Thermodynamics: Specific Heat c_p and Degree of Ionization $\langle\alpha\rangle$. In aqueous suspensions of lipids with zwitterionic headgroups, the main transition associated with the disordering of lipid acyl chains is characterized by a sharp peak in the DSC profile. A distinguishing feature of the ATR observed in the case of saturated short-chain ionic lipids is the broadening of the DSC peak, which develops into a shoulder at low ionic strengths.[14,24] Correlated with this complex DSC profile, there is an increase in the conductivity of the suspension.[23,30] A recent study that adds electrophoretic mobility data to the study of conductivity[30] yields a profile for the degree of the ionization of the lipid aqueous dispersion that presents a steep rise at the main

Table 2. Main-Transition Data for Saturated Diacyl PC Lipids,[a] Except for the Second Line (Saturated Diacyl PGs)

chain length M	12 (DL)	14 (DM)	16 (DP)	18 (DS)	20 (DA)	22 (DB)
T_m(°C)[5]	−1.9 ± 1.4	23.6 ± 1.5	41.3 ± 1.8	54.5 ± 1.5	65.3 ± 1.5	73.6 ± 2.1
T_m(°C): PGs[b]	−2	24	41.5	54.5	65	
ΔH (kcal/mol)[5]	2.1 ± 1.1	6.0 ± 2.4	8.2 ± 1.4	10.4 ± 1.6	13.3 ± 2.5	15.8 ± 2.8
a_G (Å^2)[108]	47.3[c]	47.3[c]	47.3 ± 0.3[d]	47.3 ± 0.5	47.6 ± 0.2	47.6 ± 0.2
a_F (Å^2)[109]	56.7 at 10 °C	60 at 30 °C	63.3 at 50 °C	66 at 65 °C	69.3[e]	72.42[e]
ln ω	3.896	10.175	13.123	15.973	19.775	22.930
$p = p_m$	1.948	5.087	6.561	7.986	9.887	11.465
λ	1.095	1.126	1.157	1.181	1.207	1.233
υ	4.726	4.2	3.858	3.626	3.426	3.272

[a] For all data dependent on t_m, we used the critical value $t_m = t_{crit} = 1$. [b] Main transition temperature of saturated diacyl PGs at pH 7.4 under high-ionic-strength conditions, 0.1 M NaCl.[2,125] [c] Gel areas obtained by extrapolation. [d] Comparison to DPPG gel area a_G = 48 Å^2 measured at 20 °C, pH 8.0, and 1.5 mM KCl.[126] [e] Fluid areas obtained by a linear-fitting extrapolation of the previous four points: a_F(Å^2) = 38.1 + 1.56 M.

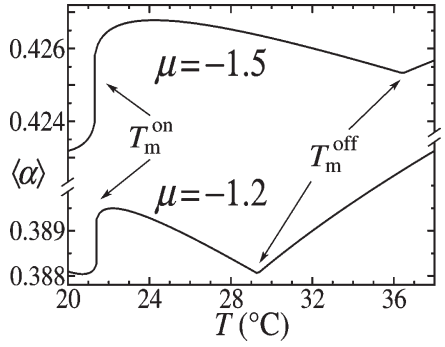

Figure 6. Thermal averaged degree of ionization $\langle\alpha\rangle$ as a function of the temperature T for $\mu = -1.5$ (top) and -1.2 (bottom). Values of the remaining parameters are p = 4.38524, λ = 1.126, ω = 6708, and υ = 4.2. Note the discontinuous chain-melting transition between two charge-ordered phases at T_m^{on} and the continuous charge-disorder transition of the fluid phase at higher temperatures T_m^{off}.

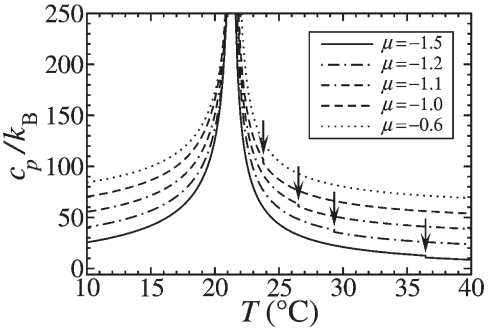

Figure 7. Specific heat at constant lateral pressure in units of k_B as a function of the temperature T for several values of the counterion chemical potential μ. The curves corresponding to different values of μ were shifted for clarity. Values of the remaining parameters are p = 4.38524, λ = 1.126, ω = 6708, and υ = 4.2. The arrows indicate the position of the second-order phase-transition temperature associated with a discontinuity in the specific-heat profile, which we interpret as the experimentally measured T_m^{off} associated with the end of the ATR.

transition, followed by increasing dissociation across the ATR, at the end of which its degree of ionization diminishes substantially.

It is then worthwhile to investigate these properties in the theoretical model system and compare them with the corresponding experimental profiles. As we show below, the statistical model reproduces some of the features of the experimental calorimetric and ionization-profile behavior of DMPG dispersions in the intermediate-salt-concentration region of the phase diagram shown in Figure 5, at which charge-ordered phases arise.

As for the model system, the predicted degree of ionization $\langle\alpha\rangle$ corresponding to the thermal average of eq 4 is shown in Figure 6. It rises discontinuously at the main transition T_m^{on}, continues to increase smoothly, and declines after a maximum down to an inflection point associated with the second-order charge-disordering transition T_m^{off}. A comparison of experiment and theory suggests the following interpretation for the ATR: at low temperatures, the ordered-chain phase also imposes headgroup charge order to lower the electrostatic energy. Thus, the entropy of the acyl chains and of the adsorbed counterions remains low. As the chain-disordering temperature T_m^{on} is attained, the headgroup separation increases abruptly, allowing for higher headgroup ionic dissociation as indicated by the steep rise in the ionization density $\langle\alpha\rangle$. The latter phase, however, keeps the charge-ordered pattern up to a higher temperature T_m^{off}, at which the charge order disappears smoothly. The broad ionization peak is thus associated with the charge-ordered headgroup fluid phase.

A second feature worth examining is the displacement of the curves for the degree of ionization $\langle\alpha\rangle$ as salt is added to the solution. Barroso and co-workers[30] have shown that as the ionic strength is lowered the $\langle\alpha\rangle$ profiles become broader, as expected, but also higher and with a larger variation range at all temperatures across the ATR interval. Model $\langle\alpha\rangle$ follows the same trend, as shown in Figure 6 for two arbitrary values of μ, although displaying variations that are an order of magnitude smaller than those suggested from the analysis of the experimental data.

The model specific heat at constant lateral pressure Π and constant chemical potential of counterions μ_c

$$\frac{1}{k_B}c_p \equiv \frac{T}{k_B}\left(\frac{\partial s}{\partial T}\right)_{\Pi,\mu_c} = -\frac{t}{J}\left(\frac{\partial^2\psi}{\partial t^2}\right)_{p,\mu} \qquad (24)$$

is shown, for different salt concentrations, in Figure 7. It can be seen that the first-order gel−fluid transition is accompanied by an apparent divergence in c_p, whereas the charge-ordered fluid phase located above T_m^{on} and below T_m^{off} contributes with a shoulder, which disappears at the charge-disordering continuous transition at higher temperatures, as indicated by the arrows in Figure 7.

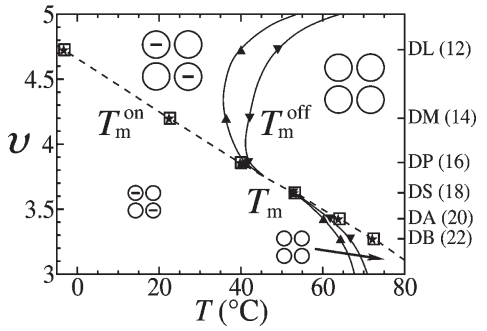

Figure 8. Phase diagram $\upsilon \times T$ for two values of the dimensionless chemical potential of counterions: $\mu = -1.5$ (□, ▲) and -2 (★, ▼). The lipid nomenclature used on the right axis is explained in footnote 34. The remaining parameter values for the several acyl-chain lengths are given in Table 2. The lines are only guides to the eyes and have the same meaning as described in the caption of Figure 3. The charge-ordered fluid phase, associated with the ATR between T_m^{on} and T_m^{off}, is broad for DLPG and DMPG, very small for DPPG, and absent for DSPG and longer chains. Note the existence of a charge-disorder continuous transition at temperatures lower than the main transition temperature T_m for longer-acyl-chain lipids DAPG and DBPG.

As for the evolution of the c_p profiles as the amount of salt (μ) increases, the sharp peak at T_m^{on} suffers a slight displacement toward higher temperatures, whereas the temperature interval at which the shoulder is seen shrinks and finally disappears. Both features reproduce the trends observed in the calorimetric measurements on DMPG aqueous suspensions upon increased ionic strength:[30] a slow rise in the first-order main transition temperature T_m^{on} and a less-gradual decrease in the ATR end at T_m^{off}.

Thus, both the ionization density $\langle\alpha\rangle$ and specific heat c_p qualitatively reproduce the behavior observed in DMPG lipid aqueous dispersions. Nonetheless, the experimental DSC shoulder is much more pronounced than the model specific-heat shoulder. Also, the variation in the model ionization density with temperature is an order of magnitude smaller than the range suggested from analysis on the basis of electrophoretic measurements.[123] A possible reason for this quantitative discrepancy could be attributed to adjustments of the aggregate conformation arising from elastic degrees of freedom[124] as well as, to lesser extent, modifications of aggregate morphology due to polymorphism, as usually observed in several single- and mixed-lipid systems.[31] We briefly discuss these points at the end of section 4.

3.4. Effect of the Saturated Diacyl-Chain Length on the ATR. In the previous subsections, we compared theoretical results with experimental data for aqueous suspensions of the saturated 14-carbon acyl-chain DMPG lipids. In this subsection, we discuss the effect of the saturated diacyl-chain length on the ATR of PGs at low ionic strength. For longer-chain lipids, such as DSPG, the ATR associated with a broadening of the DSC profile is absent, but for a somewhat shorter length, it may be very small, as for DPPG, whereas for a still shorter length it may be quite large, a few degrees as in the case of DMPG, or an even wider temperature range for DLPG.[27,37−39]

In the theoretical model, lipids with distinct acyl-chain lengths M are affected in several of their parameters, as presented in Table 2. Because ESR measurements are not available for all saturated PG lipids to perform the same fitting procedure used for DMPG in section 3.1, we will rely on known experimental data on saturated diacyl PCs.[5,108,109] This substitution can be made because in the high-ionic-strength limit saturated PGs have the same thermodynamic properties as the homologue saturated PCs with the same chain length[8,14,27,40−43] as can be endorsed by the coincidence of the first and second lines of Table 2.

On the basis of DSC measurements[5] of the main transition temperature T_m and its associated latent heat ΔH, it is possible to obtain the fluid acyl-chain degeneracy, $\omega \equiv \exp(\Delta H/k_B T_m)$, as discussed previously in connection with the Clapeyron equation (eq 23). By assuming that T_m is very close to the critical temperature of the system $T_{crit} = J/k_B$ (at the mean-field level), as previously suggested[83,91,114] and confirmed by the fitting of ESR data on DMPG in section 3.1, the lateral pressure parameter may be found by $p = p_m = (t_m/2)\ln\omega \approx {}^1/_2 \ln\omega$. The area-ratio parameter $\lambda \equiv (a_F/a_G)^{1/2}$ is given directly by estimates of the gel[108] and fluid[109] areas per lipid headgroup for saturated diacyl PCs. Finally, instead of using the bare electrostatic parameter $\upsilon_{bare} = 4t_m[l_B/(a_F)^{1/2}](T_{room}/T_m)$, which is dependent on a_F and T_m for each chain-length lipid, we multiply it by the same factor used for DMPG, $\upsilon = (420/371)\upsilon_{bare}$; see the discussion in section 3.2. We may then use the set of parameters for the different chain lengths listed in Table 2 to check the occurrence of the ATR for aqueous suspensions involving distinct chain length lipids.

The effect of the competition between hydrophobic attraction and electrostatic repulsion over the extent of the charge-ordered fluid phase for fixed values of the counterion chemical potential μ can be seen in Figure 8. As the competition parameter υ, which is proportional to the ratio of the electrostatic to hydrophobic interaction strength, decreases, the charge-ordered fluid phase, sandwiched between the charge-ordered gel and the charge-disordered fluid phases, shrinks and disappears. This feature is also compatible with the behavior of PGs,[27,37−39] which display an ATR for the shorter chains coupled to a stronger electrostatic repulsion, but none for sufficiently long chains, associated with a larger hydrophobic attraction. The electrostatic interaction strength $\tilde{V}$ due to the counterion dissociation of the PG headgroups may be taken as being independent of the acyl-chain length. Thus, the competition parameter υ may be taken as a monotonically decreasing function of the saturated diacyl-chain lengths, related to the coupling parameter J and the fluid area a_F. For the calculated transitions at finite μ, we found an almost linear relation between υ and the main transition temperature T_m, which is weakly affected by the salt concentration and follows the experimental data at high ionic strength.

4. CONCLUDING REMARKS

The main purpose of this study is the investigation of the properties of a model proposed by us previously[92] in light of the experimental data on aqueous solutions of saturated diacyl PG lipids. The latter dispersions present anomalous behavior in the case of the shorter acyl chains and under low-salt-concentration conditions, as indicated by a range of different experimental techniques. The theoretical model that we propose displays several features that may be compared to those of the experimental systems. The general properties of aqueous suspensions of dissociating lipids under variations of the acyl-chain length, salt concentration, and temperature are reproduced.

The statistical model that we propose essentially relies on the competition between hydrophobic attractions among acyl chains and electrostatic repulsions of charged headgroups. The thermodynamic analysis of the statistical model yields a framework in

which the competition sets the stage for charge ordering on lipid headgroups. The effect of the electrostatic repulsions is diluted as the hydrophobic effective van der Waals attraction increases, as for longer chain lengths. For a given ratio of the strength of the electrostatic to hydrophobic interaction, which may be associated with a given acyl-chain length, the reassociation of free counterions with charged lipid headgroups is regulated by the salt concentration and temperature.

In the case of weaker van der Waals interactions (i.e., for shorter acyl chains) and low salt concentrations, the gel−fluid main transition takes place inside the charge-ordered headgroup phase. We predict that the high DSC peak for the main transition is followed by a small shoulder, whereas the degree of dissociation develops a broad peak, as shown by DMPG aqueous suspensions. The shoulder disappears as the ionic strength is increased, whereas the maximum in the ionization of the aggregates decreases. Both features follow the experimental trend displayed by low-concentration DMPG aqueous suspensions upon the addition of salt.

In parallel, the analytical model allows us to explore the effect of the acyl-chain length under intermediate salt conditions. We were able to propose a phase diagram for the acyl-chain and headgroup lipid states for a fixed counterion chemical potential μ and different saturated diacyl-chain lengths, varying from $M = 12$ (DLPG) to 22 (DBPG).

New experimental data would be needed to provide quantitative support for the picture that we propose. Additionally, our hypothesis of charge order as a microscopic rationale for the existence of ATR would have to be experimentally tested, preliminarily for lipid monolayers, possibly through direct imaging of counterion−lipid bonding by frequency modulation AFM[127] and supplemented by the measurement of counterion profiles in the surrounding aqueous solution by X-ray standing waves.[128]

In spite of qualitative agreement between theory and experiment, a few points deserve to be stated.

(i) We have not treated the counterion and co-ion distributions in the aqueous solution. These can be accounted for by using the Poisson−Boltzmann theory[58] for ionic solutions, coupling the charged lamellar system to a reservoir of symmetric monovalent electrolyte as performed for semiphenomenological models for charged multilamellar systems,[49,50] and lamellar phases[129] or monolayers[130] composed of anion-adsorbing zwitterionic lipids. In our present approach, the effect of the electrolytic solvent is represented through a chemical potential of counterions at the lipid membrane μ_c, which of course must be in equilibrium with the chemical potential in the bulk solution. Equilibrium also requires that the latter must be constant throughout the diffuse layer. In view of this, we believe that the inclusion of the electrolytic aqueous solution contributions to the free energy should not effect substantial change in relation to the existence of headgroup-charge order. Nonetheless, it would be interesting to connect the theoretical ad hoc chemical potential of counterions μ_c to the experimental added salt concentration, beyond the ideal gas approach, and to possible ion-specific effects[82] in order to perform further quantitative tests of the theory. Ion-specific effects are indeed experimentally observed upon the addition of different monovalent counterions in aqueous suspensions of anionic lipids.[64,66−69,72,74,75]

(ii) In our theoretical model, we have assumed short-range (nearest-neighbor) electrostatic interactions among charged lipid headgroups, which allows a considerable simplification of the calculations. This assumption might be considered to be a limitation of the model and might pose doubts as to the presence of charge order in the case of more realistic long-range interactions. However, it has been shown that when one takes into account the longer-ranged interactions in a closely related model[131] the ordered phases do not disappear. Ordered configurations may be modified,[132] possibly leading to quantitatively different values of the headgroup average ionization. Thus, even if headgroup-charge ordering follows a different pattern, it should not disappear, and neither should the charge-ordered gel or the charge-ordered fluid phases.

(iii) A comparison between calorimetric and ionization density properties predicted by the theoretical model and the corresponding available experimental data points to qualitative agreement and quantitative discrepancies. The DSC shoulder and the ionization density variations are much more pronounced in the experimental data, as compared to the model theoretical predictions. A possible reason behind these discrepancies is the fact that our model does not include elastic degrees of freedom. These could be quite relevant in the case of the experimental lipid dispersions.[124] Ionization could introduce effects on morphology,[133] which could in turn enhance the charge effects. Increased curvature, for instance, may lead to increased dissociation in the fluid portions of a charged bilayer. The indication of morphological changes comes from LS data,[35,36] which suggests a substantial increment of the aggregate radius of gyration in the ATR,[134] as well as from experiments on viscosity,[30,123] which yield very large viscosities along the ATR. Pore formation on lipid vesicles has also been suggested to be a possible source of morphological change[18,24,25] and would be in line with the mutual enhancement of charge and curvature effects. However, this is a question to be more thoroughly investigated, both experimentally and theoretically.

The points raised above constitute objects of further study.

AUTHOR INFORMATION

Corresponding Authors

*E-mail: vera@if.usp.br; mtamash@ifi.unicamp.br.

Present Address

§Departamento de Física, Universidade Federal do Piauí, Centro de Ciências da Natureza, Campus Universitário Ministro Petrônio Portella, Ininga, 64049-550 Teresina, PI, Brazil.

ACKNOWLEDGMENT

This work is supported by FAPESP (Fundação de Amparo à Pesquisa do Estado de São Paulo) and CNPq (Conselho Nacional de Desenvolvimento Científico e Tecnológico).

REFERENCES

(1) (a) Nagle, J. F. *Annu. Rev. Phys. Chem.* **1980**, *31*, 157–195. (b) Nagle, J. F.; Tristam-Nagle, S. *Biochim. Biophys. Acta* **2000**, *1469*, 159–195. (c) Tristam-Nagle, S.; Nagle, J. F. *Chem. Phys. Lipids* **2004**, *127*, 3–14.

(2) Cevc, G.; Marsh, D. *Phospholipid Bilayers: Physical Principles and Models*; Wiley Interscience: New York, 1987.

(3) Marsh, D. *Chem. Phys. Lipids* **1991**, *57*, 109–120.

(4) Cevc, G., Ed. *Phospholipids Handbook*; Marcel Dekker: New York, 1993.
(5) (a) Koynova, R.; Caffrey, M. *Biochim. Biophys. Acta* **1998**, *1376*, 91–145. (b) Koynova, R.; Caffrey, M. Corrigendum. *Biochim. Biophys. Acta* **2001**, *1513*, 82.
(6) Heimburg, T. *Thermal Biophysics of Membranes*; Wiley-VCH: Weinheim, Germany, 2007.
(7) Cevc, G. *Biochim. Biophys. Acta* **1990**, *1031*, 311–382.
(8) Cevc, G. *Chem. Phys. Lipids* **1993**, *64*, 163–186.
(9) (a) Dowhan, W. *Annu. Rev. Biochem.* **1997**, *66*, 199–232. (b) Dumas, F.; Lebrun, M. C.; Tocanne, J.-F. *FEBS Lett.* **1999**, *458*, 271–277. (c) Cantor, R. S. *Biophys. J.* **1999**, *76*, 2625–2639. (d) Bezrukov, S. M. *Curr. Opin. Colloid Interface Sci.* **2000**, *5*, 237–243. (e) Dowhan, W.; Bogdanov, M. *Annu. Rev. Biochem.* **2009**, *78*, 515–540. (f) Huang, K. C.; Ramamurthi, K. S. *Mol. Microbiol.* **2010**, *76*, 822–832.
(10) (a) Lohner, K. *Development of Novel Antimicrobial Agents: Emerging Strategies*; Horizon Scientific Press: Wymondham, England, 2001. (b) Lohner, K. *Gen. Physiol. Biophys.* **2009**, *28*, 105–116.
(11) Nagle, J. F.; Scott, H. L., Jr. *Biochim. Biophys. Acta* **1978**, *513*, 236–243.
(12) Heimburg, T. *Biophys. Chem.* **2010**, *150*, 2–22.
(13) (a) Matsumoto, K. *Mol. Microbiol.* **2001**, *39*, 1427–1433. (b) Lewis, R. N. A. H.; McElhaney, R. N. *Biochim. Biophys. Acta* **2009**, *1788*, 2069–2079. (c) Roy, H. *IUBMB Life* **2009**, *61*, 940–953. (d) Prossnigg, F.; Hickel, A.; Pabst, G.; Lohner, K. *Biophys. Chem.* **2010**, *150*, 129–135.
(14) Lamy-Freund, M. T.; Riske, K. A. *Chem. Phys. Lipids* **2003**, *122*, 19–32.
(15) Riske, K. A.; Amaral, L. Q.; Lamy-Freund, M. T. *Biochim. Biophys. Acta* **2001**, *1511*, 297–308.
(16) Riske, K. A.; Amaral, L. Q.; Döbereiner, H.-G.; Lamy, M. T. *Biophys. J.* **2004**, *86*, 3722–3733.
(17) Fernandez, R. M.; Riske, K. A.; Amaral, L. Q.; Itri, R.; Lamy, M. T. *Biochim. Biophys. Acta* **2008**, *1778*, 907–916.
(18) Spinozzi, F.; Paccamiccio, L.; Mariani, P.; Amaral, L. Q. *Langmuir* **2010**, *26*, 6484–6493.
(19) Riske, K. A.; Nascimento, O. R.; Peric, M.; Bales, B. L.; Lamy-Freund, M. T. *Biochim. Biophys. Acta* **1999**, *1418*, 133–146.
(20) Riske, K. A.; Fernandez, R. M.; Nascimento, O. R.; Bales, B. L.; Lamy-Freund, M. T. *Chem. Phys. Lipids* **2003**, *124*, 69–80.
(21) Duarte, E. L.; Oliveira, T. R.; Alves, D. S.; Micol, V.; Lamy, M. T. *Langmuir* **2008**, *24*, 4041–4049.
(22) Alakoskela, J.-M. I.; Kinnunen, P. K. J. *Langmuir* **2007**, *23*, 4203–4213.
(23) Riske, K. A.; Politi, M. J.; Reed, W. F.; Lamy-Freund, M. T. *Chem. Phys. Lipids* **1997**, *89*, 31–44.
(24) Riske, K. A.; Amaral, L. Q.; Lamy, M. T. *Langmuir* **2009**, *25*, 10083–10091.
(25) Alakoskela, J.-M.; Parry, M. J.; Kinnunen, P. K. J. *Langmuir* **2010**, *26*, 4892–4900.
(26) Heimburg, T.; Biltonen, R. L. *Biochemistry* **1994**, *33*, 9477–9488.
(27) Schneider, M. F.; Marsh, D.; Jahn, W.; Kloesgen, B.; Heimburg, T. *Proc. Natl. Acad. Sci. U.S.A.* **1999**, *96*, 14312–14317.
(28) Meyer, H. W.; Richter, W.; Rettig, W; Stumpf, M. *Colloids Surf., A* **2001**, *183−185*, 495–504.
(29) Salonen, I. S.; Eklund, K. K.; Virtanen, J. A.; Kinnunen, P. K. J. *Biochim. Biophys. Acta* **1989**, *982*, 205–215.
(30) Barroso, R. P.; Riske, K. A.; Henriques, V. B.; Lamy, M. T. *Langmuir* **2010**, *26*, 13805–13814.
(31) (a) Cullis, P. R.; de Kruijff, B. *Biochim. Biophys. Acta* **1979**, *559*, 399–420. (b) Koynova, R.; Caffrey, M. *Chem. Phys. Lipids* **2002**, *115*, 107–219. (c) van Dam, L.; Karlsson, G.; Edwards, K. *Biochim. Biophys. Acta* **2004**, *1664*, 241–256. (d) Katsaras, J.; Harroun, T. A.; Pencer, J.; Nieh, M.-P. *Naturwissenschaften* **2005**, *92*, 355–366.
(32) Racey, T. J.; Singer, M. A.; Finegold, L.; Rochon, P. *Chem. Phys. Lipids* **1989**, *49*, 271–288.
(33) Kleinschmidt, J. H.; Tamm, L. K. *Biophys. J.* **2002**, *83*, 994–1003.
(34) Henceforth, we will use the conventional four-letter abbreviations for phospholipids with doubly saturated acyl chains of the form DXPY, where the second letter X labels the length of the two identical saturated acyl (or diacyl) chains of each lipid and the fourth letter Y specifies the type of polar headgroup. The lengths of the acyl chains considered in this work, measured by the number of carbon atoms, are given by L = 12 (lauroyl), M = 14 (myristoyl), P = 16 (palmitoyl), S = 18 (stearoyl), A = 20 (arachidoyl), and B = 22 (behenoyl). Examples of polar headgroups that are zwitterionic (neutral) include phosphatidylcholine (PC) and phosphatidylethanolamine (PE), whereas phosphatidylserine (PS) and phosphatidylglycerol (PG) belong to the class of anionic (negatively charged) headgroups.
(35) Enoki, T. A. Light-Scattering Characterization of Aqueous Dispersions of Anionic-Lipid Aggregates. M.S. Dissertation, Universidade de São Paulo, São Paulo, Brazil, 2010.
(36) Enoki, T. A.; Nomura, D. A.; Alves, J. R.; Henriques, V. B.; Lamy, M. T. 8th EBSA European Biophysics Congress, Budapest, Hungary; *Eur. Biophys. J.* **2011**, *40* (Suppl. 1), S200, abstract P-619. DOI: 10.1007/s00249-011-0734-z.
(37) Epand, R. M.; Gabel, B.; Epand, R. F.; Sen, A.; Hui, S.-W.; Muga, A.; Surewicz, W. K. *Biophys. J.* **1992**, *63*, 327–332.
(38) Koshinuma, M.; Tajima, K.; Nakamura, A.; Gershfeld, N. L. *Langmuir* **1999**, *15*, 3430–3436.
(39) Riske, K. A.; Barroso, R. P.; Vequi-Suplicy, C. C.; Germano, R.; Henriques, V. B.; Lamy, M. T. *Biochim. Biophys. Acta* **2009**, *1788*, 954–963.
(40) Epand, R. M.; Hui, S.-W. *FEBS Lett.* **1986**, *209*, 257–260.
(41) Kodama, M.; Miyata, T. *Colloids Surf., A* **1996**, *109*, 283–289.
(42) Koynova, R. *Chem. Phys. Lipids* **1997**, *89*, 67–73.
(43) Zhang, Y.-P.; Lewis, R. N. A. H.; McElhaney, R. N. *Biophys. J.* **1997**, *72*, 779–793.
(44) Chevalier, Y.; Zemb, T. *Rep. Prog. Phys.* **1990**, *53*, 279–371.
(45) Jusufi, A.; Hynninen, A.-P.; Haataja, M.; Panagiotopoulos, A. Z. *J. Phys. Chem. B* **2009**, *113*, 6314–6320.
(46) Moreira, L.; Firoozabadi, A. *Langmuir* **2010**, *26*, 15177–15191.
(47) Li, X.-J.; Schick, M. *Biophys. J.* **2000**, *78*, 34–46.
(48) Komura, S.; Shirotori, H.; Kato, T. *J. Chem. Phys.* **2003**, *119*, 1157–1164.
(49) Harries, D.; Podgornik, R.; Parsegian, V. A.; Mar-Or, E.; Andelman, D. *J. Chem. Phys.* **2006**, *124*, 224702.
(50) Jho, Y. S.; Kim, M. W.; Safran, S. A.; Pincus, P. A. *Eur. Phys. J. E* **2010**, *31*, 207–214.
(51) (a) Goldman, C.; Riske, K. A.; Lamy-Freund, M. T. *Phys. Rev. E* **1999**, *60*, 7349–7353. (b) Goldman, C. *J. Chem. Phys.* **2001**, *114*, 6242–6248.
(52) (a) Träuble, H.; Eibl, H. *Proc. Natl. Acad. Sci. U.S.A.* **1974**, *71*, 214–219. (b) Jähnig, F. *Biophys. Chem.* **1976**, *4*, 309–318. (c) Träuble, H.; Teubner, M.; Woolley, P.; Eibl, H. *Biophys. Chem.* **1976**, *4*, 319–342.
(53) Forsyth, P. A., Jr.; Marčelja, S.; Mitchell, D. J.; Ninham, B. W. *Biochim. Biophys. Acta* **1977**, *469*, 335–344.
(54) Watts, A.; Harlos, K.; Maschke, W.; Marsh, D. *Biochim. Biophys. Acta* **1978**, *510*, 63–74.
(55) Copeland, B. R.; Andersen, H. C. *Biochemistry* **1982**, *21*, 2811–2820.
(56) (a) Gouy, G. *C. R. Acad. Sci.* **1909**, *149*, 654–657. (b) Gouy, G. *J. Physique (Paris)* **1910**, *9*, 457–468. (c) Gouy, G. *Ann. Phys. (Paris)* **1917**, *7*, 129–184.
(57) Chapman, D. L. *Philos. Mag.* **1913**, *25*, 475–481.
(58) (a) Israelachvili, J. N. *Intermolecular and Surface Forces*, 2nd ed.; Academic Press: London, 1992; pp 213−259. (b) Andelman, D. Electrostatic Properties of Membranes: The Poisson−Boltzmann Theory. In *Handbook of Biological Physics*; Lipowsky, R., Sackmann, E., Eds.; Elsevier: Amsterdam, 1995; Vol. 1B, pp 603−641. (c) Netz, R. R.; Orland, H. *Eur. Phys. J. E* **2000**, *1*, 203–214. (d) Deserno, M.; Holm, C. Cell Model and Poisson−Boltzmann Theory: A Brief Introduction. In *Proceedings of the NATO Advanced Study Institute on Electrostatic Effects in Soft Matter and Biophysics*; Holm, C., Kékicheff, P., Podgornik, R.,

Eds.; Kluwer: Dordrecht, The Netherlands, 2001; pp 27−50. (e) Safran, S. A. *Statistical Thermodynamics of Surfaces, Interfaces and Membranes*; Addison-Wesley: Reading, MA, 1994; pp 153−167. (f) Tamashiro, M. N.; Schiessel, H. *Phys. Rev. E* **2003**, *68*, 066106. (g) Lamm, G. *Rev. Comput. Chem.* **2003**, *19*, 147–365. (h) Grochowski, P.; Trylska, J. *Biopolymers* **2007**, *89*, 93–113.

(59) Stern, O. *Z. Elektrochem.* **1924**, *30*, 508–516.

(60) (a) Meijer, L. A.; Leermakers, F. A. M.; Nelson, A. *Langmuir* **1994**, *10*, 1199–1206. (b) Pandit, S. A.; Berkowitz, M. L. *Biophys. J.* **2002**, *82*, 1818–1827. (c) Gurtovenko, A. A.; Vattulainen, I. *J. Phys. Chem. B* **2008**, *112*, 4629–4634.

(61) (a) Kaznessis, Y. N.; Kim, S.; Larson, R. G. *Biophys. J.* **2002**, *82*, 1731–1742. (b) Murzyn, K.; Róg, T.; Pasenkiewicz-Gierula, M. *Biophys. J.* **2005**, *88*, 1091–1103. (c) Elmore, D. E. *FEBS Lett.* **2006**, *580*, 144–148. (d) Pickholz, M.; Oliveira, O. N., Jr.; Skaf, M. S. *Biophys. Chem.* **2007**, *125*, 425–434. (e) Zhao, W.; Róg, T.; Gurtovenko, A. A.; Vattulainen, I.; Karttunen, M. *Biophys. J.* **2007**, *92*, 1114–1124. (f) Zhao, W.; Róg, T.; Gurtovenko, A. A.; Vattulainen, I.; Karttunen, M. *Biochimie* **2008**, *90*, 930–938. (g) Yi, M.; Nymeyer, H.; Zhou, H.-X. *Phys. Rev. Lett.* **2008**, *101*, 038103. (h) Hénin, J.; Shinoda, W.; Klein, M. L. *J. Phys. Chem. B* **2009**, *113*, 6958–6963.

(62) Kurland, R.; Newton, C.; Nir, S.; Papahadjopoulos, D. *Biochim. Biophys. Acta* **1979**, *551*, 137–147.

(63) Toko, K.; Yamafuji, K. *Chem. Phys. Lipids* **1980**, *26*, 79–99.

(64) Lakhdar-Ghazal, F.; Tichadou, J.-L.; Tocanne, J.-F. *Eur. J. Biochem.* **1983**, *134*, 531–537.

(65) Garidel, P.; Blume, A. *Chem. Phys. Lipids* **2005**, *138*, 50–59.

(66) Eisenberg, M.; Gresalfi, T.; Riccio, T.; McLaughlin, S. *Biochemistry* **1979**, *18*, 5213–5223.

(67) Lakhdar-Ghazal, F.; Tocanne, J.-F. *Biochim. Biophys. Acta* **1988**, *943*, 19–27.

(68) Loosley-Millman, M. E.; Rand, R. P.; Parsegian, V. A. *Biophys. J.* **1982**, *40*, 221–232.

(69) Hauser, H.; Shipley, G. G. *Biochemistry* **1983**, *22*, 2171–2178.

(70) Kinoshita, M.; Kato, S.; Takahashi, H. *Chem. Phys. Lipids* **2009**, *161*, 1–10.

(71) (a) Cevc, G.; Watts, A.; Marsh, D. *FEBS Lett.* **1980**, *120*, 267–270. (b) Cevc, G.; Watts, A.; Marsh, D. *Biochemistry* **1981**, *20*, 4955–4965.

(72) Eklund, K. K.; Salonen, I. S.; Kinnunen, P. K. J. *Chem. Phys. Lipids* **1989**, *50*, 71–78.

(73) Tamashiro, M. N.; Henriques, V. B.; Lamy, M. T. *Langmuir* **2005**, *21*, 11005–11016.

(74) Eklund, K. K.; Virtanen, J. A.; Vuori, K.; Patrikainen, J.; Kinnunen, P. K. J. *Biochemistry* **1987**, *26*, 7542–7545.

(75) Kraayenhof, R.; Sterk, G. J.; Sang, H. W. W. F.; Krab, K.; Epand, R. M. *Biochim. Biophys. Acta* **1996**, *1282*, 293–302.

(76) Marra, J. *Biophys. J.* **1986**, *50*, 815–825.

(77) Lotta, T. I.; Salonen, I. S.; Virtanen, J. A.; Eklund, K. K.; Kinnunen, P. K. J. *Biochemistry* **1988**, *27*, 8158–8169.

(78) Yang, Y.; Mayer, K. M.; Hafner, J. H. *Biophys. J.* **2007**, *92*, 1966–1974.

(79) McLaughlin, S. *Annu. Rev. Biophys. Biophys. Chem.* **1989**, *18*, 113–136.

(80) Egorova, E. M. *Colloids Surf., A* **1996**, *110*, 47–53. Egorova, E. M. *Colloids Surf., A* **1998**, *131*, 7–18. Egorova, E. M. *Colloids Surf., A* **1998**, *131*, 19–31.

(81) (a) Lyklema, J. *Colloids Surf., A* **2006**, *291*, 3–12. (b) Lyklema, J. *Adv. Colloid Interface Sci.* **2009**, *147−148*, 205–213.

(82) (a) Travesset, A.; Vaknin, D. *Europhys. Lett.* **2006**, *74*, 181–187. (b) Travesset, A.; Vangaveti, S. *J. Chem. Phys.* **2009**, *131*, 185102.

(83) Doniach, S. *J. Chem. Phys.* **1978**, *68*, 4912–4916.

(84) Caillé, A.; Pink, D.; de Verteuil, F.; Zuckermann, M. J. *Can. J. Phys.* **1980**, *58*, 581–611.

(85) Mouritsen, O. G.; Boothroyd, A.; Harris, R.; Jan, N.; Lookman, T.; MacDonald, L.; Pink, D. A.; Zuckermann, M. J. *J. Chem. Phys.* **1983**, *79*, 2027–2041.

(86) Jerala, R.; Almeida, P. F. F.; Biltonen, R. L. *Biophys. J.* **1996**, *71*, 609–615.

(87) Kharakoz, D. P.; Panchelyuga, M. S.; Tiktopulo, E. I.; Shlyapnikova, E. A. *Chem. Phys. Lipids* **2007**, *150*, 217–228.

(88) Sugár, I. P.; Thompson, T. E.; Biltonen, R. L. *Biophys. J.* **1999**, *76*, 2099–2110.

(89) Michonova-Alexova, E. I.; Sugár, I. P. *Biophys. J.* **2002**, *83*, 1820–1833.

(90) Mouritsen, O. G. *Chem. Phys. Lipids* **1991**, *57*, 179–194.

(91) (a) Nielsen, L. K.; Bjørnholm, T.; Mouritsen, O. G. *Nature* **2000**, *404*, 352. (b) Nielsen, L. K.; Bjørnholm, T.; Mouritsen, O. G. *Langmuir* **2007**, *23*, 11684–11692.

(92) Tamashiro, M. N.; Barbetta, C.; Germano, R.; Henriques, V. B. *Phys. Rev. E* **2011**, *84*, 031909; DOI: 10.1103/PhysRevE.84.031909. This paper presents calculations performed on the fully equivalent mean-field model in the Curie−Weiss[93] formulation.

(93) (a) Thompson, C. J. *Classical Equilibrium Statistical Mechanics*; Clarendon Press: Oxford, England, 1988; pp 91−95. (b) Salinas, S. R. A. *Introduction to Statistical Physics*; Springer-Verlag: New York, 2001; pp 266−268.

(94) (a) Helm, C. A.; Laxhuber, L.; Lösche, M.; Möhwald, H. *Colloid Polym. Sci.* **1986**, *264*, 46–55. (b) Hauser, H. *Chem. Phys. Lipids* **1991**, *57*, 309–325.

(95) Besides their extended and ordered acyl chains, PG lipids in the gel phase usually arrange in a regular orthorhombic lattice.[43,77,96] However, depending on the preparation conditions, the chains in the gel phase may also adopt a hexagonal packing,[96] as more commonly observed in the gel phase of zwitterionic lipids.

(96) (a) Ranck, J. L.; Keira, T.; Luzzati, V. *Biochim. Biophys. Acta* **1977**, *488*, 432–441. (b) Garidel, P.; Richter, W.; Rapp, G.; Blume, A. *Phys. Chem. Chem. Phys.* **2001**, *3*, 1504–1513.

(97) We do not treat amphoretic systems, in which an uncharged counterion-associated site may adsorb an additional cation or an anion, leading to a possible charge inversion of the surface. Charge order/disorder in this class of systems, which contain both oppositely charged species, has been investigated experimentally and/or theoretically: (a) Meyer, E. E.; Lin, Q.; Hassenkam, T.; Oroudjev, E.; Israelachvili, J. N. *Proc. Natl. Acad. Sci. U.S.A.* **2005**, *102*, 6839–6842. (b) Perkin, S.; Kampf, N.; Klein, J. *J. Phys. Chem. B* **2005**, *109*, 3832–3837. (c) Perkin, S.; Kampf, N.; Klein, J. *Phys. Rev. Lett.* **2006**, *96*, 038301. (d) Naydenov, A.; Pincus, P. A.; Safran, S. A. *Langmuir* **2007**, *23*, 12016–12023. (e) Brewster, R.; Pincus, P. A.; Safran, S. A. *Phys. Rev. Lett.* **2008**, *101*, 128101. (f) Sarabadani, J.; Naji, A.; Dean, D. S.; Horgan, R. R.; Podgornik, R. *J. Chem. Phys.* **2010**, *133*, 174702. (g) Naji, A.; Dean, D. S.; Sarabadani, J.; Horgan, R. R.; Podgornik, R. *Phys. Rev. Lett.* **2010**, *104*, 060601. (h) Baytekin, H. T.; Patashinski, A. Z.; Branicki, M.; Baytekin, B.; Soh, S.; Grzybowski, B. A. *Science* **2011**, *333*, 308–312. (i) In particular, it has been proposed in part h that the underlying physical mechanism behind the very old problem of contact electrification in dielectric materials is the development of a random mosaic of oppositely charged regions of nanoscopic dimensions. Additionally, closest to the ionogenic system investigated here, ion-induced segregation yielding neutral or undissociated gel-like domains in a charged fluid background has been experimentally observed in mixed monolayers of zwitterionic PC and anionic PG lipids in the presence of divalent counterions[98] and in DPPG monolayers in the presence of monovalent[99] and divalent counterions.[100]

(98) Evert, L. L.; Leckband, D.; Israelachvili, J. N. *Langmuir* **1994**, *10*, 303–315.

(99) Grigoriev, D.; Krustev, R.; Miller, R.; Pison, U. *J. Phys. Chem. B* **1999**, *103*, 1013–1018.

(100) Grigoriev, D.; Miller, R.; Wüstneck, R.; Wüstneck, N.; Pison, U.; Möhwald, H. *J. Phys. Chem. B* **2003**, *107*, 14283–14288.

(101) It is possible to attribute different energies for individual lipids with acyl chains in the gel and fluid states, ε_G and ε_F, respectively. This inclusion is straightforward, and it has been considered in ref 92. The main results remain the same; this just changes the definition of $\Delta\varepsilon$ in eq 9 (see eq 6 in ref 92).

(102) (a) Bragg, W. L.; Williams, E. J. *Proc. R. Soc. London, Ser. A* **1934**, *145*, 699–730. (b) Bragg, W. L.; Williams, E. J. *Proc. R. Soc. London,*

Ser. A **1935**, *151*, 540–566. (c) Williams, E. J. *Proc. R. Soc. London, Ser. A* **1935**, *152*, 231–252.

(103) (a) Hill, T. L. *An Introduction to Statistical Thermodynamics*; Dover: New York, 1986; pp 246−252. (b) Huang, K. *Statistical Mechanics*, 2nd ed.; John Wiley: New York, 1987; pp 352−357. (c) Thompson, C. J. *Classical Equilibrium Statistical Mechanics*; Clarendon Press: Oxford, England, 1988; p 135. (d) Pathria, R. K. *Statistical Mechanics*, 2nd ed.; Butterworth-Heinemann: Oxford, 1996; pp 321−327. (e) Salinas, S. R. A. *Introduction to Statistical Physics*; Springer-Verlag: New York, 2001; pp 263−266.

(104) Although it might be tempting to give a physical interpretation of the several terms in eq 12, for example, to associate the logarithmic terms to entropic contributions and the remaining terms to energetic (or enthalpic) ones, we should stress that this idea is utterly misleading, as discussed for the simplest case of the standard ferromagnetic Ising model in Carneiro, C. E. I.; Henriques, V. B.; Salinas, S. R. *Physica A* **1989**, *162*, 88–98.

(105) However, p must lie in the interval $(\lambda-1)v/4 < p < p_{crit} = {}^1/_2 \ln \omega$ such that there is no critical point for finite μ.

(106) For the interested reader, the existence of both acyl-chain-order discontinuous transitions as well as charge-order continuous transitions is discussed at the end of section V.A in ref 92.

(107) (a) Lee, T. D.; Yang, C. N. *Phys. Rev.* **1952**, *87*, 410–419. (b) Baxter, R. J. *Exactly Solved Models in Statistical Mechanics*, 3rd printing; Academic Press: London, 1989; pp 24−30. (c) Stanley, H. E. *Introduction to Phase Transitions and Critical Phenomena*; Clarendon Press: Oxford, England, 1971; pp 260−264.

(108) Sun, W.-J.; Tristram-Nagle, S.; Suter, R. M.; Nagle, J. F. *Biophys. J.* **1996**, *71*, 885–891.

(109) Petrache, H. I.; Dodd, S. W.; Brown, M. F. *Biophys. J.* **2000**, *79*, 3172–3192.

(110) Bloch, J. M.; Yun, W. *Phys. Rev. A* **1990**, *41*, 844–862.

(111) Incidentally, one should mention that a proper definition of the mechanical lateral pressure Π for unilamellar vesicles is a nontrivial question: (a) Tanford, C. *Proc. Natl. Acad. Sci. U.S.A.* **1979**, *76*, 3318–3319. (b) White, S. H. *Proc. Natl. Acad. Sci. U.S.A.* **1980**, *77*, 4048–4050. (c) Lis, L. J.; McAlister, M.; Fuller, N.; Rand, R. P.; Parsegian, V. A. *Biophys. J.* **1982**, *37*, 667–672. (d) Feng, S.-s. *Langmuir* **1999**, *15*, 998–1010. (e) Marsh, D. *Langmuir* **2006**, *22*, 2916–2919. (f) Fournier, J.-B.; Barbetta, C. *Phys. Rev. Lett.* **2008**, *100*, 078103. (g) Barbetta, C.; Imparato, A.; Fournier, J.-B. *Eur. Phys. J. E* **2010**, *31*, 333–342.

(112) (a) Blume, A. *Biochim. Biophys. Acta* **1979**, *557*, 32–44. (b) Marsh, D. *Biochim. Biophys. Acta* **1996**, *1286*, 183–223.

(113) This fitted set of dimensionless parameters, however, does not determine the original energy density (eq 2) model parameters (Π, ε_{FF}, ε_{GG}, ε_{GF}) unambiguously. Further results, for example, those obtained by atomistic simulations, or hypotheses need to be considered. However, to analyze the thermodynamic model properties, a knowledge of these individual parameters is not necessary.

(114) (a) Marčelja, S. *Biochim. Biophys. Acta* **1974**, *367*, 165–176. (b) Morrow, M. R.; Whitehead, J. P.; Lu, D. *Biophys. J.* **1992**, *63*, 18–27.

(115) Callen, H. B. *Thermodynamics and an Introduction to Thermostatistics*, 2nd ed.; John Wiley: New York, 1985; pp 228−231.

(116) Bjerrum length calculated by using the experimentally measured water dielectric constant $\varepsilon_W = 78.38$ at 25° C and 0.1 MPa. Archer, D. G.; Wang, P. *J. Phys. Chem. Ref. Data* **1990**, *19*, 371–411.

(117) These might include contributions from charged neighbors at longer separations, ionic screening due to the mobile free ions,[118] the presence of dielectric contrast between the aqueous solvent and the acyl-chain region,[118−120] and hydration effects.[121,122]

(118) Netz, R. R. *Phys. Rev. E* **1999**, *60*, 3174–3182.

(119) (a) Levin, Y. *Phys. Rev. Lett.* **2009**, *102*, 147803. (b) Levin, Y.; dos Santos, A. P.; Diehl, A. *Phys. Rev. Lett.* **2009**, *103*, 257802. (c) dos Santos, A. P.; Diehl, A.; Levin, Y. *Langmuir* **2010**, *26*, 10778–10783. (d) dos Santos, A. P.; Levin, Y. *J. Chem. Phys.* **2010**, *133*, 154107.

(120) Tamashiro, M. N.; Constantino, M. A. *J. Phys. Chem. B* **2010**, *114*, 3583–3591.

(121) Cevc, G.; Marsh, D. *J. Phys. Chem.* **1983**, *87*, 376–379.

(122) Ben-Yaakov, D.; Andelman, D.; Podgornik, R. *J. Chem. Phys.* **2010**, *134*, 074705.

(123) Barroso, R. P. Dimyristoyl Phosphatidylglycerol Lipid Dispersions: A Thermo-Structural Study. Ph.D. Thesis, Universidade de São Paulo, São Paulo, Brazil, 2010.

(124) (a) Lipowsky, R. *Nature* **1991**, *349*, 475–481. (b) Sackmann, E. *FEBS Lett.* **1994**, *346*, 3–16. (c) Claessens, M. M. A. E.; van Oort, B. F.; Leermakers, F. A. M.; Hoekstra, F. A.; Stuart, M. A. C. *Biophys. J.* **2004**, *87*, 3882–3893. (d) Marsh, D. *Chem. Phys. Lipids* **2006**, *144*, 146–159.

(125) Cevc, G. Thermodynamic Parameters of Phospholipids. In *Phospholipids Handbook*; Cevc, G., Ed.; Marcel Dekker: New York, 1993; Appendix B, Table B1, p 939.

(126) Watts, A.; Harlos, K.; Marsh, D. *Biochim. Biophys. Acta* **1981**, *645*, 91–96.

(127) Fukuma, T.; Higgins, M. J.; Jarvis, S. P. *Phys. Rev. Lett.* **2007**, *98*, 106101.

(128) Bedzyk, M. J.; Bommarito, G. M.; Caffrey, M.; Penner, T. L. *Science* **1990**, *248*, 52–56.

(129) Leontidis, E.; Aroti, A.; Belloni, L.; Dubois, M.; Zemb, T. *Biophys. J.* **2007**, *93*, 1591–1607.

(130) Leontidis, E.; Aroti, A.; Belloni, L. *J. Phys. Chem. B* **2009**, *113*, 1447–1459.

(131) Tröster, A. *Phys. Rev. B* **2010**, *81*, 012406.

(132) (a) Oitmaa, J. *J. Phys. A: Math. Gen.* **1981**, *14*, 1159–1168. (b) Landau, D. P.; Binder, K. *Phys. Rev. B* **1985**, *31*, 5946–5953.

(133) (a) Kumaran, V. *Phys. Rev. Lett.* **2000**, *85*, 4996–4999. (b) Sung, W.; Choi, E.; Kim, Y. W. *Phys. Rev. E* **2006**, *74*, 031907. (c) Taheri-Araghi, S.; Ha, B.-Y. *Langmuir* **2010**, *26*, 14737–14746.

(134) Spongelike connected networks[26,27,38] proposed earlier to explain the ATR behavior have been ruled out through experimental verification of the stability of closed and nonmerging bilayer aggregates.[14,22,24,35,36] Proposed bilayer fragments or bicelles[28] must also be discarded, in light of strong evidence of the preserved spherical symmetry of the vesicular aggregates along the ATR.[35,36]

NOTE ADDED AFTER ASAP PUBLICATION

This article was published ASAP on September 15, 2011. A new version was published on September 22, 2011, with changes to equation 9. An additional text change has been made in section 2. STATISTICAL MODEL AND THERMODYNAMICS: CHAIN AND HEADGROUP CHARGE ORDERING. The correct version was published on October 25, 2011.